EVALUATING THE VARIABLES THAT IMPACT

ULTRASONIC TESTING

A thesis presented to the Faculty of the Graduate School at the University

of Missouri – Columbia

In Partial Fulfillment of the Requirements for the

Degree of Master of Science

---

by

DANIEL WAYNE LOOTEN

Dr. Glenn Washer, Graduate Advisor

JULY 2014

The undersigned, appointed by the Dean of the Graduate School, have examined the thesis entitled:

EVALUATING THE VARIABLES THAT IMPACT

ULTRASONIC TESTING

Presented by **Daniel Wayne Looten**

A candidate for the degree of **Master of Science**,

And hereby certify, in their opinion, it is worthy of acceptance.

_____

Professor Glenn Washer

_____

Professor Brent Rosenblad

_____

Professor Roger Fales

ACKNOWLEDGEMENTS

TABLE OF CONTENTS

iv

LIST OF FIGURES

LIST OF TABLES

LIST OF APPENDICIES

ABSTRACT

The goal of this research was to improve the quality control process for steel fabrication to improve the reliability, safety and quality of welded steel components. The objectives of this project were to explore the relationship between the capabilities of ultrasonic testing (UT) and phased array ultrasonic testing (PAUT) and the requirements for flaw detection and characterization. This research assessed the variables that impact UT measurements to improve the methodology used to inspect steel welds in structural components.

This research explored the variables that influence the ultrasonic response to improve which include: length measurement, beam spread, attenuation, defect orientation, transducer rotation, wedge angle and defect sizing. The results from these tests were then compared to the American Welding Society (AWS) UT procedure used to inspect structural components in steel bridges. The findings from the length measurement test indicated that defects smaller than the transducer were typically oversized. The results from the defect orientation and wedge angle tests indicated that the defect's orientation and the wedge angle greatly affected the reflected amplitude. The results from the attenuation tests indicated that the assumptions made in AWS acceptance criteria were inaccurate.

The results from this research will then be used in the development of PAUT. This thesis contains test procedures developed for PAUT. The PAUT procedures will evaluate the variables measured in this research for UT. The results from the PAUT tests will then be used to develop a procedure for PAUT inspection.

1 INTRODUCTION

1.1 Goal and Objectives

The goal of the research reported herein was to improve the quality control process for steel fabrication to improve the reliability, safety and quality of welded steel components. The objectives of this research were to

- Measure key factors that influence ultrasonic testing (UT) measurements.

- Assess the influence of these factors on the American Welding Society UT procedure used to detect and characterize defects.

- Identify improvements to current UT procedures.

- Develop test procedures to assess these key factors for phased array ultrasonic testing (PAUT) measurements.

This project explored the relationship between the capabilities of these technologies and the requirements for flaw detection and characterization. This research assessed UT technologies to improve the methodology used to inspect steel welds in structural components.

This thesis explored the use of UT to detect defects within steel welds. UT is used to evaluate welded regions of steel members for subsurface flaws during fabrication as well as in the field. UT incorporates high frequency acoustic waves to detect and assess defects in welds. The effectiveness of UT relies on the interpretation of acoustic waves reflected from these defects. Defect

features, such as orientation and surface roughness can affect the ultrasonic response, which results in inaccurate representations of the defects within the measurement results. PAUT incorporates the same mechanics to inspect welded components; however, PAUT inspection procedures have not been developed to inspect building or bridge components. This research explores the variables that influence the ultrasonic response to improve the reliability of UT measurements. Test procedures for PAUT were also designed to measure these variables for future research. The results from the future work would then be used to develop inspection procedures for building and bridge components using PAUT.

1.2 Sherman-Minton Bridge

The Sherman Minton Bridge (SMB), shown in Figure 1-1, was opened in 1961 and carries I-64 traffic across the Ohio River from Kentucky to Indiana. The 5-span bridge includes two simple span steel tied arch trusses that are considered fracture critical. The SMB carries an average daily traffic of approximately 80,000 vehicles. The bridge was inspected using nondestructive evaluation (NDE) technologies between April 2011 and October 2011. The bridge was subsequently closed for 5 months, during which time the bridge was strengthened to mitigate the risk of fracture. (Gorrill 2011). On September 8, 2011, a significant vertical crack was identified in one of the fracture critical tie girders, shown in Figure 1-2.

Figure 1-1: Sherman Minton Bridge (Stone and Green 2011)

The SMB was evaluated using multiple NDT technologies, during the inspection, including: magnetic particle testing (MT), radiographic testing (RT) and UT (Hotaki and Washer 2014). The results from these inspections indicated discrepancies between the different NDE technologies. A single, highly reliable NDE technology would be preferred in bridge inspections rather than multiple conflicting technologies which yield conflicting test results.

Figure 1-2: Vertical crack located in the SMB arch tie butt weld.

The effectiveness of the NDT technologies is affected by the reliability of the results. The vertical defect that resulted in the SMB closing was identified and evaluated correctly; however, the results from other NDT tests on the bridge were inconsistent. Subsurface defects that were detected using ultrasonic testing went undetected in the RT tests and vice-versa (Hotaki and Washer 2014). NDT technologies and testing procedures must provide accurate and consistent results when evaluating subsurface defects. The studies described in Section 2.3 of this report have evaluated the reliability of NDE technologies capable of detecting subsurface defects such as RT, UT and PAUT. These reliability studies considered not only the number of missed defects, or "false negatives", but also how many times the inspectors detected a defect that was not present or a "false positive".

The present research addresses the need to develop updated testing procedures for ultrasonic and phased array testing. The research focuses on key

parameters that affect UT measurements to assess the influence of these parameters on test results. The application of the suggested updates to the current procedure could potentially improve the reliability of UT and/or PAUT in identifying defects within steel welds.

1.3 Scope

Reliable quality control methods are required in the construction of steel elements for new and more efficient bridge designs. UT is a traditional quality control procedure for welding, coupled with RT for critical applications. However, the UT methods traditionally applied are highly variable and the reliability of these methods is uncertain. This research developed UT technologies to improve the safety and quality of welded constructions. The research explored the relationship between the capabilities of the technology and requirements for flaw detection and characterization.

In order to test the capabilities of UT and PAUT, test specimens with idealized flaws were assessed using traditional ultrasonic technologies. Specimens were also fabricated with embedded flaws typically encountered during the fabrication and welding process. Additional test specimens were developed to assess key factors that impact ultrasonic response for both UT and PAUT.

1.4 Existing Technologies and Their Limitations

This section describes other technologies used to inspect steel welds in steel bridge components. These technologies inspect the welds for defects such

as slag, heat affected cracks, and fatigue cracks that develop into discontinuities large enough to cause failure. There are several NDT technologies that are used to identify defects in steel welds including: RT, MT, and dye penetrant.

RT is a method in which X-Ray or gamma rays are used to identify defects within steel welds (ASTM 2010). Similar to UT, RT is capable of detecting subsurface defects in steel welds. The process consists of exposing the weld to high energy photons emitted from a radiation source. The dense steel material absorbs the high energy protons while defects and discontinuities allow the photons to pass through. A film or cassette is placed on the opposite side of the weld material to record the photons that pass through the volume of the weld. The result is a two-dimensional projection of the steel weld onto the film with defects represented by dark dark areas on the film. Defects on the film appear darker due to the difference in the absorbed energy on the film.

The advantage of using RT is that the test results yield an image of the defect that can be interpreted: however, the effectiveness of RT is limited by the orientation and size of the defect (Rana, Hedden et al. 2001). Defects normal to the two-dimensional film are difficult for RT to detect because the resulting image on the radiograph may appear as a very small dot or simply does not show up at all.   Small cracks elude RT because they do not develop voids within the material large enough to appear on the radiograph. UT is often paired with RT to compensate for these limitations. RT is a high-priced NDT technology due to the expensive equipment and materials used. Unlike the other NDT, the use of RT

has certain health risks associated with prolonged exposure to the radiation used during the test (Murthy 1998).

MT is a method in which surface-breaking defects are identified through the use of metal shavings and induced magnetic fields (ASTM 2008). Unlike UT, MT is only effective in evaluating surface defects. The procedure entails spreading metal shavings across the steel weld. Two magnets are placed on the surface of the steel. The two magnets induce a magnetic field in the steel that leaks from the surface at the defect. The magnetic particles are then attracted to the defect, forming a line of magnetized particles along the length of the defect on the surface of the weld material.

While MT is effective in identifying surface cracks, it is limited in its ability to detect subsurface defects. The benefits of MT are its low cost and limited required training to perform the test.

Dye penetrant inspection, or liquid penetrant inspection, can also be used to detect surface-breaking cracks (ASTM 2012). Similar to MT, dye penetrant inspection cannot detect subsurface defects. The process begins by cleaning the weld of any dust and dirt using a cleaner or remover compound. Colored dye penetrant is then spread across the weld surface and seeps into any surface cracks or surface porosity. The excess penetrant is wiped off the steel surface, but the penetrant that drained into the cracks remains. Once the weld is cleaned, a developer is sprayed on to the weld. The surface tension of the liquid penetrant causes the penetran to be drawn from the crack. Defects are identified by the colored penetrant that rises to the surface of the weld and contrasts with

the developer.   While surface-breaking cracks can be identified with dye penetrant, this process cannot identify characteristics such as depth or subsurface length.

1.5 Discussion

All NDT technologies have unique limitations.   Some technologies are unable to detect subsurface defects, while other technologies are ineffective in evaluating certain types of defects.   In order to compensate for the limitations of a single technology, bridges similar to the Sherman-Minton Bridge are sometimes inspected using several different NDT technologies.   While the use of multiple technologies complement each other and account for the unique limitations of each technology, the combined results from the technologies may conflict with one another (Hotaki and Washer 2014).   It is important to use technologies that are capable of not only detecting defects throughout the entire weld volume but are also accurate in defect characterization.

Ultrasonic testing is capable of detecting and characterizing subsurface defects within steel welds.   Compared to the other technologies, UT is the preferred technology when inspecting welds for subsurface cracks.   While UT is adequate for detection purposes, studies show high variability between technician reports with respect to defect characterization.   PAUT is a newer technology that has been designed to improve inspection reliability in regards to defect characterization.   PAUT improves upon angle beam UT by increasing the amount of information gathered from each scan.   The PAUT scans provide

images in the form of sectorial or S-Scans. These images are similar to the images produced in a medical sonogram. PAUT scans can be used to better determine defect characteristics. PAUT may soon be preferred to UT because defects are easier to identify using the PAUT imaging. In order to assess the effectiveness of UT and PAUT, it is important to identify the limitations of each technology and improve upon current ultrasonic procedures.

2 BACKGROUND

This chapter describes background information on UT and PAUT. This background information includes describing the use of beam angles in traditional UT, beam angles used for PAUT, and characteristics of sound fields produced by typical ultrasonic transducers. Key parameters that affect these sounds fields, and consequently impact UT results, are described in this section.

The chapter also discusses ultrasonic code procedures published by the American Welding Society (AWS), the American Society of Mechanical Engineers (ASME) and the American Petroleum Institute (API). These codes describe commonly used UT procedures used for quality control and in-service inspection in different fields of engineering. These procedures are included to provide an overview of different approaches to using UT to detect defects in engineering structures.

Prior work regarding UT and its use for defect detection is described in Section 2.3. Included in this section is a description of prior research to explore key parameters that affect UT results. These key parameters affect the reliability of the test method, because typical variations in the parameters cause differences in the interpretation of test results. Consequently, tests may yield different outcomes for the same situation, depending on variations in these parameters and human factors. Previous testing on the reliability of UT is described to illustrate the impact of these variations on UT results. Comparison of the UT approach with alternatives of PAUT and RT is also described.

2.1 Ultrasonic Measurement Theory

This section describes briefly the mechanics behind UT. UT and PAUT apply ultrasonic theories for the purpose of detecting and characterization defects within materials (Krautkrämer and Krautkrämer 1990, Lamarre, Moles et al. 2000). In these approaches, acoustic waves are generated by a transducer and propagate into a material under test. Reflections of the wave occur at discontinuities in the material such as a defect or a boundary, and are detected by the transducer. These reflected waves (i.e. signals) are interpreted to detect and characterize defects.

Transducers used for traditional UT consist of a piezoelectric crystal enclosed within a plastic or stainless steel housing. The piezoelectric crystals expand when electrically charged, thus generating an acoustic wave (Curie and Curie 1880). When the piezoelectric crystal is compressed, a small electric potential is generated. The waves reflected from defects within the material travel back to the transducer and compress the piezoelectric crystal. The piezoelectric crystal then generates an electric potential with an amplitude relative to the intensity of the reflected wave. The reflected amplitude is displayed in an A-Scan on an oscilloscope which displays the time at which the wave was received and the wave amplitude.

2.1.1 Angle Beam Ultrasonic Testing

Both straight beam and angle beam transducers are used in the inspection of steel structures. Straight beam transducers send the acoustic wave

11

into the material at an incidence angle of 0°. The straight beam transducers are not effective when evaluating welds that were not ground flush because the coarse weld surface obstructs the wave generated by the straight beam transducer.   In order to avoid the coarse weld surface an acrylic wedge is attached to the transducer to angle the acoustic wave.   These angle beam ultrasonic transducers are used to inspect the entire volume of the weld without significant weld preparation.

An angle beam transducer uses a shear wave propagating through the material being inspected. The transducer generates a longitudinal wave into the acrylic wedge; however, the angle beam ultrasonic transducer relies on only the shear wave to inspect the weld.   The acoustic wave is manipulated using an acrylic wedge which causes the longitudinal wave to propagate at or near its critical angle with the steel, allowing primarily the shear wave to propagate into the steel as shown in Figure 2-1. Because the longitudinal wave is at or near its critical angle, the reflected amplitude is negligible.   The critical angle for the longitudinal wave and the shear wave angle can be calculated using Snell's Law equations below:

$$\frac{\sin(\theta_1)}{c_1} = \frac{\sin(\theta_2)}{c_2} \qquad\qquad \text{Equation } 2.1 - 1$$

Where:

θ_1 and θ_2 are the angles of incidence for the material and,

c_1 and c_2 are the wave velocities based on the speed of sound within the materials and the wave types.

12

There are two main types of angle beam ultrasonic testing: time of flight diffraction (TOFD) testing and pulse echo testing. The TOFD technique requires two angle beam probes during inspection. One probe sends the angled acoustic wave into the material, and the other transducer receives the waves that propogate through the material or are diffracted by internal discontinuities (Silk 1977, Charlesworth and Temple 1989). Internal discontinuities are characterized based on the times of flight for the received signals.

This research focuses on the pulse echo technique which requires a single probe that generates and receives the reflected wave (Firestone 1942, Desch, Sproule et al. 1946). Figure 2-1 illustrates the wave paths of the shear and longitudinal waves from a single ultrasonic transducer. The pulse echo technique is typically preferred for bridge inspection because it only requires access to a single weld side, unlike TOFD, which requires access to both sides.
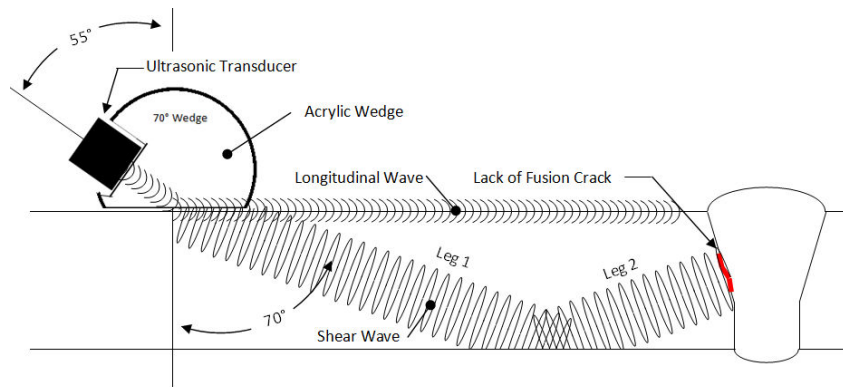
Figure 2-1: Wave path of a 70° angle beam wedge transducer

Figure 2-1 also depicts the "legs" that refer to different wave path regions. The first wave path region is located between the point at which the wave enters the steel and the point where it reflects off the opposite (back) side of the steel.

13

The second leg refers to the region where the wave reflects off the back of the steel to where the wave reflects off the top surface of the steel.

2.1.2 Phased Array Ultrasonic Testing

Phased array ultrasonic testing (PAUT) incorporates ultrasonic theory to generate an image, known as an S-Scan (ASTM 2009). S-Scans evaluate multiple incidence angles and display the reflected amplitude corresponding to each angle. The traditional angle beam ultrasonic transducer consists of a single oscillator whose acoustic wave is manipulated by an acrylic wedge. A phased array probe consists of several separately wired oscillators, or elements, positioned along a single row, or array, within the transducer. An angle beam PAUT probe used to inspect steel welds typically includes a minimum of 16 elements (ASTM 2013). The resolution of the S-Scan improves based on the number of elements in the probe.
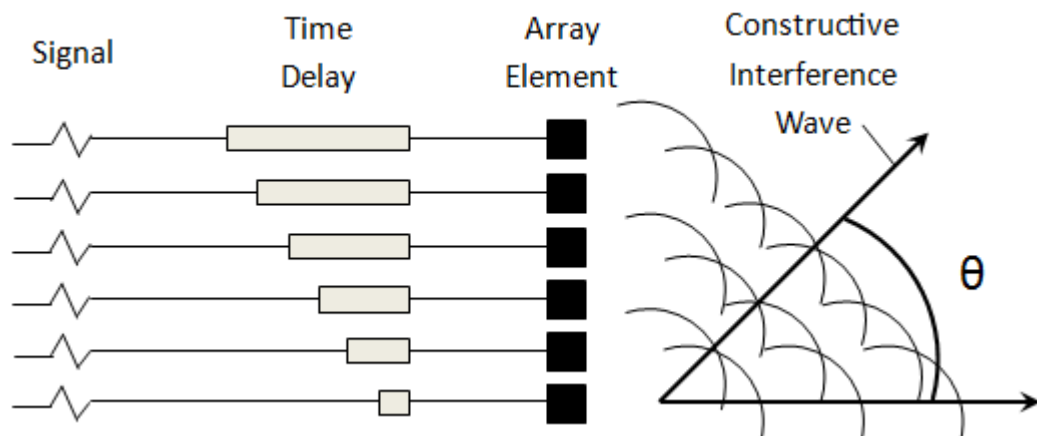
Figure 2-2: Phased array ultrasonic testing wave propagation

The PAUT transducer generates a wave of constructive interference to form an angled beam (Song, Shin et al. 2002). This process is known as

14

"steering." Figure 2-2 shows a schematic diagram of beam steering using time delay. Each element is stimulated with a different time delay resulting in constructive interference. The resulting wave is used to inspect the weld. The steering angle, θ, is controlled using different time delays. This process is rapidly repeated, changing the steering angle to each angle in the desired range, such as 40°-75°. The PAUT receiver stores information on the reflected amplitude to include time, angle and amplitude. This information is used to generate an S-Scan. This S-Scan displays the amplitude represented by a color located at a given reflection angle and reflection time. Figure 2-3 shows the constructive interference waves propagating from the phased array transducer to the defect. The phased array receiver is capable of generating A-Scans associated with each angle as described in Section 3.2. Using the PAUT, defects are much easier to detect, and multiple A-scans can be assessed in a single scan.
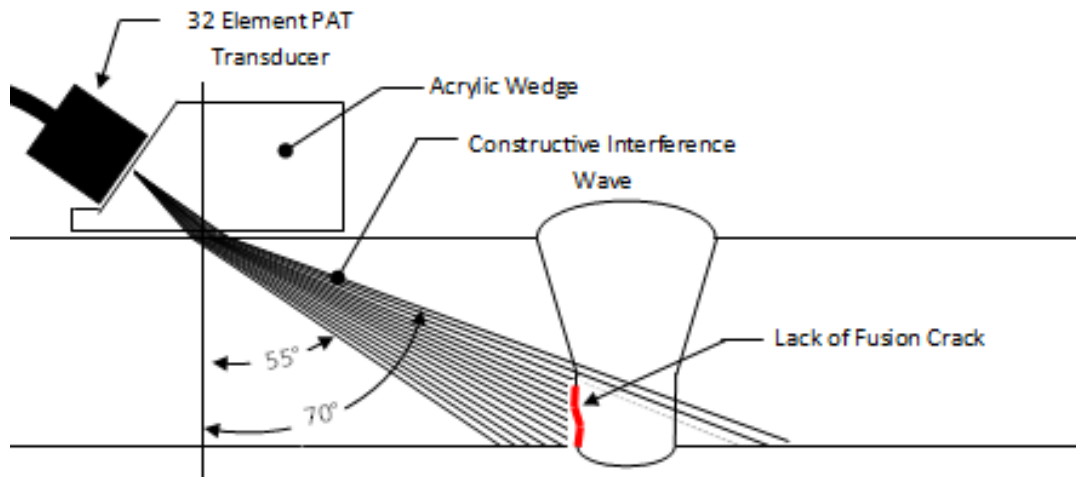
Figure 2-3: Shear wave path of a 32 element, PAUT transducer

2.1.3 Sound Field

This section describes the sound field as the acoustic wave propagates through the material. Ultrasonic waves are generated from the transducer and transmit through the material. The material properties and geometry affect how the wave travels through the material. The following sections describe the parameters that affect the wave behavior and how the ultrasonic testing results are impacted.

The term "sound field" refers to the behavior of ultrasonic waves as the waves propagate through the material prior to encountering any defects. Once the acoustic wave reflects off a defect and echoes back to the transducer, the wave behavior is known as the "echo field". Figure 2-4 shows the two regions in each sound field: the near field and the far field. The near field is a region that contains interference due to the various wave pressures resulting from the initial pulse. These wave pressures propagate through the material based on the transducer's oscillator geometry. The near field starts at the beginning of the sound field and ends at the last interference point. The far field region begins at the end of the near field region. This region is ideal for defect inspection because it does not contain any wave pressure interference.
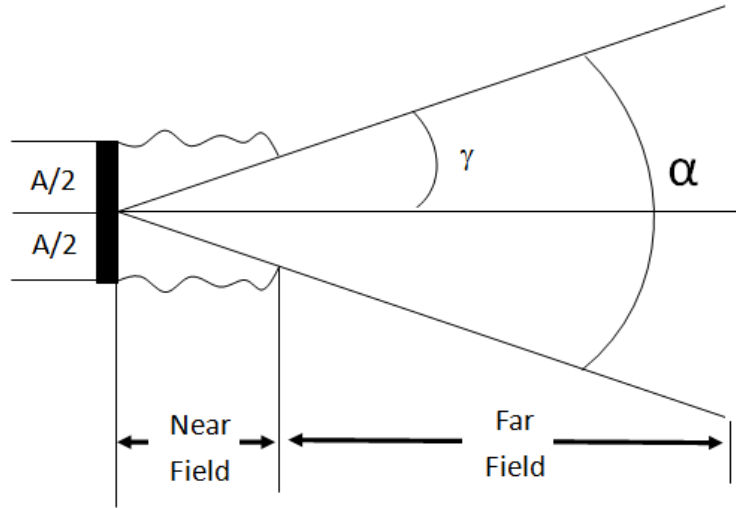
Figure 2-4: Sound field diagram

The interference contained within the near field results from the interaction between wave pressure maxima and minima. The near field is calculated from the oscillator geometry and the acoustic beam wavelength. The ratio of the oscillator diameter, D, to the wavelength, λ, determines the number of maxima and minima within the near field. The path difference between the waves reaches an exact multiple of λ and identifies the maxima sound pressure. The position of the last pressure maximum on the axis depends on D and λ in accordance with the relationship:

$$N = \frac{D^2 - \lambda^2}{4\lambda}$$
Equation 2.1-1

For this research, a square transducer is used during testing. Due to the rectangular geometry of the transducer, the near field length calculation is as follows:

$$N = h\left(\frac{a^2}{\lambda}\right)$$
Equation 2.1-2

17

where *h* is derived from the relationship between the sides of the transducer (b/a ratio) and is found in Table 1. This research utilizes a 0.625" x 0.625" transducer, so b/a is equal to 1.00 and *h* is 1.37.

Table 1: Values of factor *h* of rectangular piston oscillators

Ratio of sides b/a	h
1.0	1.37
0.8	1.15
0.6	1.04
0.4	1.00
0.2	0.99

As seen in Figure 2-4, the far field begins at the end of the near field. As the wave propagates into the material the wave disperses into the material to form the beam spread shown in Figure 2-4. Figure 2-4 shows the beam spread starting at the center of the oscillator and propagating into the material. The rectangular oscillator has two edges, Side 1 and Side 2. These edges have different lengths, *A* and *B*, respectively. The beam spread angle is different for each of these axes. The following equations are used to determine the angle of divergence, γ, or half the beam spread angle, α, for each axis:

$$\sin(\gamma_1) = k_{dB} * \left(\frac{2*\lambda}{A}\right)$$ Equation 2.1.2-3

$$\sin(\gamma_2) = k_{dB} * \left(\frac{2*\lambda}{B}\right)$$ Equation 2.1.2-4

The constant, k_{dB}, is related to a defined amplitude drop. In the AWS code, a -6dB drop in the echo field is used in the length measurement, so k_{dB} from Table 2 is 0.44.

18

Table 2: Values of factor k_{dB} for a given dB drop

Free Field		k_{dB}	Echo Field	
A	ΔdB		α	ΔdB
0.84	-1.5	0.32	0.71	-3.0
0.71	-3.0	0.44	0.50	-6.0
0.50	-6.0	0.60	0.25	-12.0
0.32	-10.0	0.74	0.10	-20.0
0.00	-∞	1.00	0.00	-∞

2.1.4 Attenuation

As the acoustic wave propagates through the material, the wave energy disperses into the material (Krautkrämer and Krautkrämer 1990). The scattering and absorption of the wave energy into the material is known as attenuation. The amplitude loss due to attenuation is calculated using the following equation:

$$A = A_0 e^{-\alpha d} \hspace{4cm} \text{Equation 2.1.3-1}$$

Where A is the reduced amplitude due to attenuation at a given distance, d, and A_0 is the initial amplitude, and α is the attenuation coefficient associated with the material. The attenuation coefficient can be calculated using the following equation:

$$\alpha = \frac{0.1151}{v} U_t \hspace{4cm} \text{Equation 2.1.3-2}$$

where v is the wave speed of the material. U_t is determined by evaluating two adjacent reflections and determining the change in decibels divided by the amount of time between the reflections.

19

2.2 Ultrasonic Testing Code Procedures

This section describes the AWS, ASME and API inspection codes used to evaluate engineering structures. The AWS ultrasonic testing procedure is used in the inspection of steel bridge and building welds. The ASME ultrasonic testing procedure is used to evaluate welded mechanical components such as pressure vessels. The API ultrasonic testing procedure is used to inspect pipeline welds. Each ultrasonic testing procedure has unique criteria for items such as calibration and defect measurement.

In order to limit the amount of human error and improve quality control, the codes require technicians to meet training requirements prior to conducting any inspections. Technicians are categorized into three levels (Level I, II and III), each required to complete a certain number of field inspection hours and pass a series of written comprehensive exams. Level I technicians are permitted to conduct UT inspections designed by Level III technicians and are supervised by Level II and III technicians. Level II technicians are capable of calibrating the equipment and are permitted to evaluate test results. The Level II technicians must follow the procedures provided by the Level III technician or provided in the UT code. The Level III technicians are able to train Level I and II technicians, and develop UT procedures used by the lower level technicians.

2.2.1 AWS Ultrasonic Testing Procedure

The American Welding Society (AWS) developed the AWS D1.1 and AWS D1.5 codes for the inspection of building and bridge components,

respectively (AWS 2010, Bridge Welding Code 2010). Each code provides step-by-step ultrasonic testing procedures used by Level I or higher technicians. These ultrasonic testing procedures are used in the inspection of steel welds during the fabrication process as well as in the field. The AWS ultrasonic procedure provides a detailed UT procedure in which all welds must meet a standard acceptance criterion. The AWS Code requires the contractor responsible for inspecting the structure to prepare a report containing: the welds to be tested, location of the defects, and corresponding drawings that define the testing parameters.

The AWS ultrasonic testing procedure requires that the volume of the weld is examined using angle beam transducers. For angled beam tests, the sensitivity of the transducer is calibrated using either an approved calibration block such as an IIW calibration block or a sensitivity calibration block as described in Section 3.3.5. The transducer is calibrated by adjusting the gain to the horizontal reference level of 80% full screen height (FSH) from the 0.06 inch side drilled hole in the calibration block. The gain at which the receiver is set to attain reflected amplitude of 80% FSH is recorded as zero reference level, "b".

In order to inspect the entire volume of the weld, the AWS ultrasonic code provides three angle beam probes, 45°, 60° and 70°. AWS code identifies which angle beam probe should be used to inspect for the top quarter, middle half and bottom quarter of each weld. The necessary probes are determined based on the thickness of the weld. Planar defects oriented parallel to the UT wave path

may elude UT. In order to account for these planar defects, all welds are inspected from multiple sides to inspect all possible defects from multiple angles.

Once detected, all indications are further evaluated to determine the maximum attainable amplitude. The gain is adjusted so that the maximum amplitude is at 80% FSH. The new gain value is reported in decibels as the Indication Rating, "a." The AWS accounts for the loss in amplitude due to attenuation by including an Attenuation Factor, "c" in the indication rating. The Attenuation Factor is found by subtracting 1 inch from the wave path length, multiplying the remainder by 2 and rounding it to the nearest dB level. The Indication Rating, "d," is compared to the acceptance criteria provided in the AWS code to determine each indication's severity and is calculated using the following equations.

Instruments with gain in dB: $a - b - c = d$ **Equation 2.2.1-1**

Instruments with attenuation in dB: $b - a - c = d$ **Equation 2.2.1-2**

This research uses an instrument with gain, so Equation 2.2.1-1 was used. The indication rating is compared to the acceptance criteria listed in the AWS code to determine the discontinuity severity class. The classes range from Class D (minor discontinuity) to Class A (major discontinuity). Class A defects are characterized as unacceptable, while the acceptance for the other classes is based on the indication rating and the defect's measured length. The AWS code associates the edge of each crack with a 50% (6 dB) drop from the maximum attainable amplitude. The crack edge location corresponds to the transducer centerline location at which the defect indication decreases to 50% maximum

amplitude. The flaw length is determined by measuring the distance between these centerline locations for both crack edges. If the defect length is larger than the allowable length, the defect is rejected.

2.2.2 ASME Ultrasonic Testing Procedure

The American Society of Mechanical Engineers (ASME) developed the ASME Section V: Nondestructive Examination code which contains guidelines for ultrasonic testing of mechanical components (ASME 2011). The ASME code does not provide a step-by-step procedure for ultrasonic testing; however, the code provides guidelines used by Level III inspectors to develop manual and automated examination procedures. The code contains details and procedure qualifications for straight beam, angle beam and phased array ultrasonic testing as well as qualifications for search unit spacing based on beam spread, attenuation and scanning sensitivity. These procedures are used to inspect welds and compare any indications found to the project's pre-determined acceptance criteria.

Both the straight beam and angled beam transducers are used to inspect the volume of each weld. The straight beam probes are used to inspect the base material for defects, while the angled beam probes are used to inspect the weld volume. The angle beam search unit is typically 45° but can be angled appropriately for the weld configuration. The angle beam transducer is oriented perpendicularly to the weld to detect defects parallel to the weld. Similar to the AWS, this test is repeated on both sides of the weld to detect defects oriented

parallel to the wave path. In order to detect defects transverse to the weld, the angle beam transducer is placed on the weld and angled parallel to the weld axis. The search unit is then rotated 180° and the examination is repeated. If the weld is not ground flat, this test is performed in the base material, on both sides of the weld, in each direction.

The ASME ultrasonic testing code addresses the effects of beam spread in the automated probe qualification section. In order to ensure the entire weld volume is inspected, transducers must be spaced so that a minimum of 10% scanning overlap is attained. In order to determine the overlap from each transducer, a calibration block as seen in Figure 2-6 is used to determine the left/right and towards/away beam spread angles.

FIG. B-466   BEAM SPREAD
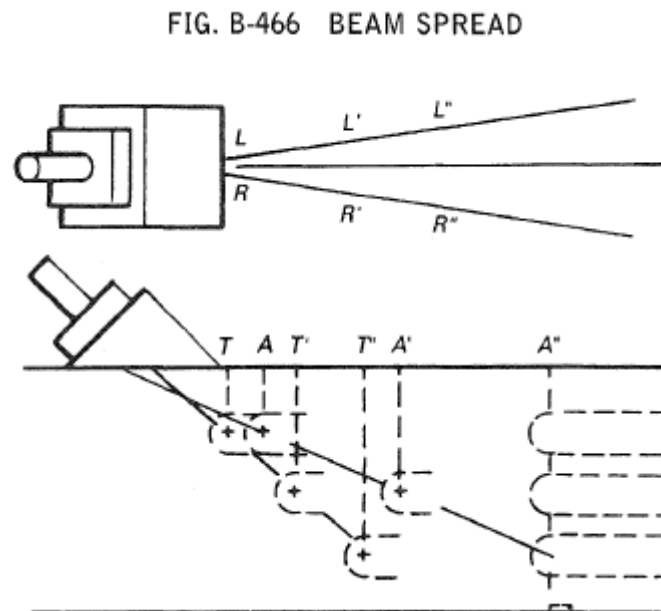
Figure 2-5: Beam spread calibration of the ASME Ultrasonic Code

Three rounded bottom holes located at 1/4, 1/2 and 3/4 of the calibration block thickness are inspected. The maximum reflected amplitude from each

24

round bottom hole is first identified. T, T' and T'' shown in Figure 2-5 refer to the locations at which the maximum reflected amplitude drops by 50% as the transducer moves toward the round bottom hole. This process is repeated by moving the probe left, right and away from the rounded bottom holes. The A locations and the T locations are used to calculate the vertical beam angle, and the L locations and R locations are used to calculate the horizontal beam angle. The beam angles are then used to determine the required transducer spacing for each probe.

The ASME code uses a distance amplitude correction (DAC) curve to develop a reference level as seen in Figure 2-6. The DAC curve is developed using the maximum reflected amplitude from side drilled holes of similar diameter at different depths. The indications are of similar sized holes; however, the reflected amplitude decreases due to the material attenuation. These indications are used to develop a reference line used to determine a defect's acceptance or rejection. If any measured indication is larger than the DAC curve, the indication represents a defect larger than the side drilled hole at that depth. Any defect that is 20% of the DAC curve is further characterized and compared to the acceptance criteria. During the initial inspection, the ASME code requires that the sensitivity level is set 6 dB or higher than the reference level to ensure all possible defects are detected. These indications are then further evaluated to establish their severity.
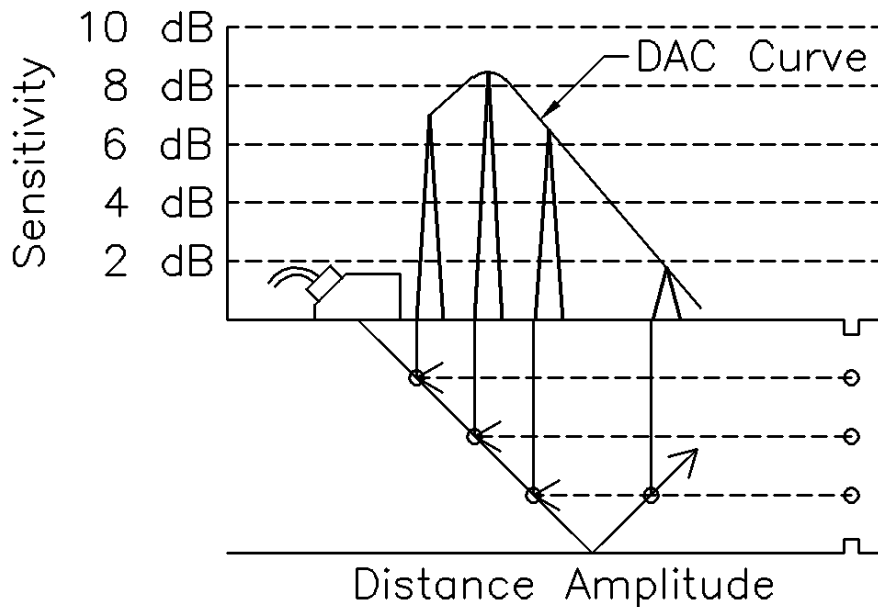
Figure 2-6: DAC curve construction

2.2.3 API Ultrasonic Testing Code

The American Petroleum Institute (API) code for ultrasonic testing is used by piping companies and ultrasonic contractors to develop acceptable ultrasonic examination procedures (Standard 2005). The code contains details and procedure qualifications for straight beam, angle beam and phased array ultrasonic testing. This code is used by the ultrasonic contractor to develop ultrasonic procedures for each pipeline. The contractor is required to demonstrate the proposed procedures to the piping company and produce acceptable and accurate results. The results from these procedures are compared to the piping company's acceptance criteria. These procedures are then used to ensure quality in the steel welds during the fabrication process and as well as inspect welds currently in the field.

26

All inspections are developed by an NDT Level III UT technician. Only Level II and Level III NDT inspectors are allowed to calibrate the equipment and interpret the results. Each inspection is required to include the following: weld type, material type, surface preparation, stage at which evaluation was performed, instruments used, couplant type and testing technique. In describing the testing technique, it is required that the transducer wedge angle, frequencies, material temperature scanning patterns as well as inspection speed, defect location (datum), reference standards, calibration requirements and sensitivity in decibels are included.

The API incorporates a DAC curve to account for the loss in reflected amplitude due to attenuation. Calibration blocks include two notches located at the top and bottom of the block. Both notches have a depth of 10% calibration block thickness. These upper and lower notches are used to develop a DAC curve similar the curve mentioned in Section 2.2.2.

The manual procedure requires that the scanning sensitivity is set at 6 dB or more than the DAC reference sensitivity, similar to the ASME code. All indications that exceed the DAC + 6dB limit are evaluated. The reference, scanning and defect evaluation sensitivity are incorporated into the final report to determine the defect's severity. All of the observed defects are compiled in an ultrasonic testing report and presented to the piping company. Using the defect information from the UT report, the piping company is then responsible for determining the quality of the weld.

2.3 Prior Work

This section contains three sections describing the prior work related to different areas of UT inspection. The first section describes prior work that evaluated the variables that impact the ultrasonic measurement results. The second section describes prior work containing performance evaluations of UT technicians. The third section focuses on studies that compare the effectiveness of the NDT technologies capable of inspecting subsurface defects: RT, UT and PAUT.

2.3.1 Ultrasonic Response Variables

As described in Section 2.2.1, the AWS ultrasonic acceptance criterion incorporates the measured defect length and the maximum reflected amplitude to determine the defect's severity. This section describes prior research on variables that impact the length and amplitude measurements. These factors include: defect angle, beam spread, surface roughness and defect texture.

The NCHRP 242 report evaluated the effect of attenuation and the effect of transducer angle on the reflected amplitude (Meyer 1984) (Jessop, Mudge et al. 1981). The AWS assumes defects are oriented vertically because a vertical crack is the most severe orientation for defects. The report found that the AWS code estimates a decrease in amplitude of 3 dB between measurements made using a 45° and 60° transducers and a decrease of 2 dB between measurements 60° and 70° transducers. The report also indicated that the reflected amplitude decreases as the transducer is rotated about the defect. The highest amplitude

was observed when the transducer was oriented perpendicular to the defect. The reflected amplitude decreased at a slower rate for small defects, but large defects showed a greater loss in reflected amplitude as the transducer was rotated about the defect.

A study conducted by the Federal Highway Administration demonstrated the effects of beam spread on the measured defect length as the wave path length increases (Moore, Phares et al. 2004). A side drilled hole 0.039 inch in diameter was inspected using UT, creating B-Scans at several wave path lengths. B-Scans refer to an inspection in which the transducer location is associated with the defect's reflected amplitude. The results determined that beam spread impacted the length measurement for defects smaller than the transducer. The results showed that the measured defect length increased with increased wave path length.

Nagy and Rose evaluated the effect of contact surface roughness scattering when inspecting subsurface defects (Nagy and Rose 1993). They determined that the scattering effect is determined by the transducer frequency and the material roughness. They found that high frequency waves are absorbed into the material more severely and are affected considerably by contact surface roughnesses. The large contact surface roughness created greater wave scattering and interference in high frequency transducers than when using low frequency transducers. Low frequency waves used in AWS ultrasonic transducers travel through the small roughnesses and propogate through the material. The roughnesses evaluated in this research were small

(smooth to 43 µin) and demonstrated noise interference on high frequency transducers.

The same theory and principles used to estimate the effects of contact surface roughness on reflected amplitude can also be applied to find the impact that subsurface defect roughness has on the reflected amplitude (Ogilvy 1989). Crutzen et al conducted a study to evaluate realistic defects within steel welds (Crutzen, Lemaitre et al. 1996, Wirdelius and Österberg 2000). The study inspected specimens containing three types of defects: smooth cracks with sharp crack edges, rough cracks and volumetric defects, such as slag and porosities. The results indicated that small rough defects were easier to detect than small smooth defects, but also found that the scattering associated with rough defects also complicated defect characterization.

2.3.2 UT Reliability

This section describes studies that look at the reliability of ultrasonic testing. Due to the nature of nondestructive testing, test results are often never conclusive. Most inspections are not confirmed by destructively sampling the inspected specimen to confirm test results. Because these tests lack confirmation, it is important to determine the reliability of all NDT technologies. The reliability of a technology is determined by the likelihood of zero false indications while detecting all defects located in the material. False indications, or "false positives," refer to nonexistent defects reported by an operator. False positives increase the total cost of renovating a bridge, and excessive false

30

positives may result in an unnecessary termination of the bridge. Missed indications, or "false negatives," may result in the failure of the component.

Prior to the inspection of the Sherman Minton Bridge, a performance test was conducted to ensure that the inspectors were providing consistent and accurate results in the identification and characterization of defects within steel welds. The operators were instructed to follow procedures based on the AWS D1.5 code to inspect test specimens containing known defects. The maximum reflected amplitude, the flaw length and the flaw location were recorded and analyzed. The results were then compared using a reliability rating system developed in prior UT research (Washer, Connor et al. 2013).

The results of the performance test revealed inconsistencies in the reported amplitudes and flaw length measurements. Error as a percentage of flaw length was greatest (110%) for the short flaw, and least for the longest flaw (15%). It was concluded from these results that the UT procedure generally overestimated the length of small flaws, and its accuracy increased as the flaw length increased. Results from the UT testing also revealed that "repeat calls", where an indication is reported more than once, occurred several times during the testing.

The effectiveness of UT relies on the diligence and experience of each technician and varies between technicians. For example, Gruber and Light tested the reliability of inspectors using the AWS D1.1 Code to assess welded moment frame joints. Twelve mockup specimens containing a total of 20 flaws were inspected by two qualified inspectors. Results were assessed to determine

the number of known flaws not detected by the inspectors, or "missed indications", as well as indications reported where no flaw exists, or "false alarms". Results showed 4 missed indications and 13 false alarms (Gruber and Light 2002). Shaw performed a similar reliability evaluation on UT technicians in which 15 UT technicians inspected 12 welds with embedded defects. In total, there were 222 tests on known flaws, with 56 missed indications, 166 detections, and 32 false alarms (Shaw Jr 2002).

The NCHRP 242 report contained a study which evaluated 14 known flaws which had been assessed by 3 different inspectors. The inspectors rated the flaws according to the AWS procedure for acceptable or reject able indications. Eight flaws were rejected by all inspectors (58%); there was disagreement on the accept/reject decision for five of the flaws (35%) (Jessop, Mudge et al. 1981). Additionally, the amplitude rating measured during the testing varied on average 6.5 dB; This results indicates high variability in a key parameter which used accept or reject as a given indication.

2.3.3 Comparing RT, UT and PAUT

This section describes studies conducted that compared the effectiveness of the NDT technologies capable of detecting subsurface flaws. The technologies evaluated in these studies were RT, UT and PAUT. It is important to compare the effectiveness of each technology to determine the best technology suited for defect characterization. UT and PAUT use the same theory to detect defects. As a result, the NDT industry has accepted PAUT as a

suitable replacement for UT. PAUT offers more efficient scans which provide several angles of inspection compared to the single angle of inspection generated by UT. The following studies were conducted to evaluate the capability of both UT and PAUT to identify and characterize defects in order to establish PAUT as a suitable replacement for UT.

A study conducted by the ASME has considered using only UT for crack detection purposes (Rana, Hedden et al. 2001). While UT is effective in detecting planar defects, or crack-like defects, RT is much less effective. In order to detect defects using RT, a large change in volume, or void, is required. Planar defects may not contain a large void, but other defects such as porosity and slag are easily detected using RT. From a fracture analysis standpoint, the most critical orientation for a defect in a steel weld is a vertically oriented defect. Due to the orientation and defect type, RT is ineffective in evaluating these defects. This study concluded that UT is more reliable than RT in detecting subsurface cracks, and the procedure and technology must be improved to ensure greater reliability in UT inspection results.

Ditchburn et al. addressed the differences between UT and PAUT as well as some of the difficulties associated with transitioning from UT to PAUT (Ditchburn and Ibrahim 2009). He found that PAUT decreased inspection time by increasing inspection coverage and sensitivity. The array of elements used in PAUT produce an S-scan comprised of multiple A-scans at different angles. For example, a PAUT transducer is able to inspect the 45°-70° angles in a single scan, and is capable of inspecting the defect at all three standard AWS

33

transducer angles at once. The resulting S-scan displays multiple inspection angles allowing easier defect detection; however, the increase in inspection angles also leads to more complicated results that require a higher level of interpretation. This study concluded that while proper training would resolve any interpretation issues, there is still a need for acceptable inspection standards for PAUT.

The Florida Department of Transportation conducted tests to determine the effectiveness of RT, UT and PAUT (Wilkinson and Duke 2014). The purpose of the study was to establish the effectiveness of PAUT and eventually to include PAUT in the AWS D1.5 inspection code. Each of the technologies was used to inspect steel bridge weld samples. The data found it was uncommon for RT to detect defects that UT and PAUT did not detect. They also found that there were no instances in which PAUT rejected a defect that UT and RT found acceptable. These results indicate that UT and PAUT are capable of identifying nearly every defect RT can identify. It also indicates that PAUT did not report additional false indications relative to the UT and RT results. Since the rejection rate for each technology was similar (PAUT 8.7%, UT 7.4%, and RT 9.3%), it was concluded that PAUT would be acceptable for inspecting steel bridge welds. In order to obtain the most accurate inspection results, the PAUT procedure would include a supplemental manual to evaluate edge cracks and transverse defects.

3   EXPERIMENTAL PROCEDURES

This chapter describes the experimental testing procedures used during this research. Section 3.1 describes the procedures conducted in this research that determined the variables that impact the ultrasonic measurement. These procedures evaluated sound field characteristics, including beam spread, attenuation and wedge angle.   Other procedures evaluated defect characteristics, including defect orientation and defect texture. The remaining test procedures assessed the inspection process by evaluating the effects of transducer orientation and the length measurement procedures. Both fabricated slots in test specimens and defects within a steel weld were examined using the AWS length measurement procedure. These variables impacted the reflected amplitude and length measurement used in ultrasonic testing to identify and characterize defects within steel welds.

The remaining sections describe the acquired data format, the testing equipment and the test specimens that were inspected.   The data formats resulting from these test procedures are described in Section 3.2.   Each test procedure required testing equipment including AWS transducers, an encoder, a puler-receiver and a LabView program were used in the data collection. The test equipment is described in Section 3.3.   The test procedures in Section 3.1 required manufactured test specimens to be manufactured. The test specimens include: FBH1, LA1, SR1, fatigue specimens and the SMB11 plate. The unique properties of each test specimen are described in Section 3.4.

3.1 Test Procedures

This section describes the test procedures conducted to measure the variables that impact ultrasonic measurements. These tests evaluate variables that impact ultrasonic measurements. The procedures also determine the consistency and repeatability of the current ultrasonic testing procedures. Table 3 is a test matrix that lists the test procedures, the inspected test specimens, the purpose of the test and the number of tests conducted for each procedure.

Table 3: Test Matrix

Procedure	Test Specimen	Purpose of Test	# of UT Tests
Length Measurement	LA1	Test to determine effectiveness of amplitude related defect sizing	160
Defect Texture	SR1, Fatigue Specimens	Test to determine effect of defect texture on reflected amplitude	80
Subsurface Defect Orientation	LA1	Test to determine effect of defect orientation on reflected amplitude	30
Transducer Orientation	SDH1, LA1	Test to determine effect of transducer orientation on reflected amplitude	40
Wedge Angle	LA1, SR1	Test to determine effect of wedge angle on reflected amplitude	60
Beam Spread	LA1	Test to determine effect of beam spread on the reflected amplitude	162
Attenuation	LA1, SR1	Test to determine effect of attenuation on the reflected amplitude	65
Defect Sizing	SMB 11	Test to determine effectiveness of amplitude related defect sizing	60

3.1.1 Subsurface Defect Texture

The subsurface defect texture test evaluated the reflected amplitude from specimens containing different wall surface finishes. As stated in Section 2.2.1, a major component in the AWS ultrasonic testing procedure acceptance criteria is the reflected amplitude. The reflected amplitude reportedly indicates the defect size, but does not account for any interference caused by the defect's

texture. The reflected amplitude may not be the same for a smooth slag inclusion as it would be for a rough fatigue crack of the same size. It is important to identify the interference associated with both types of defect textures and adjust the acceptance criteria to account for these differences.

In order evaluate subsurface discontinuities with known textures, steel specimens with walls containing different surface finishes were inspected. The SR1 shown in Figure A-4 to Figure A-10, contains 8 sides with different surface finishes. The results from the SR1 sides were then compared to sides from fatigued specimens to relate the collected data from the SR1 to reflected amplitudes from realistic defect textures. The fatigue specimens shown in Figure A-11 to Figure A-17 were provided by Purdue University. These fatigue specimens represent indications similar to defects found in in-situ welds.

The defect texture tests inspected the walls of both the fabricated specimens and the fatigue specimens. B-Scans were created during the inspection of the fabricated specimens by moving the transducer along each SR1 wall length while inspecting an area located 0.75" deep on each wall. Due to the geometry of the fatigue specimen, B-Scans were not effective. Instead, multiple A-Scans were taken to identify the reflected amplitude from the fatigued sides. The thin thickness of the fatigue specimen reflected both wall corners in the A-Scan wave forms. The reflected amplitude for each fatigued side was assumed to be located between both corner reflections. The maximum amplitude was determined in this region and the results were compared to the fabricated specimen results.

3.1.2 Length Amplitude

The length measurement tests evaluated the accuracy of the 6 dB drop technique used in the AWS code to characterize defects. As stated in Section 2.2.1, a major component in the AWS ultrasonic testing procedure acceptance criteria is the defect's length measurement. The defect's edges are associated with a 6 dB drop in reflected amplitude. This does not account for beam spread or for defects with lengths shorter than the transducer.

The results from the Sherman-Minton Bridge performance evaluation found that when the defect length is smaller than the size of the transducer, the measured length is much longer than the actual defect length. When the transducer scans a defect smaller than the transducer, the entire defect is encompassed in the transducer scan as seen in Figure 3-1. The defect is completely encompassed in the scan, resulting in an extension of length at which maximum amplitude is attained. During inspection, the reflected amplitude is averaged over the area of the oscilator, if the defect is encompassed by the transducer over a length of 0.1", then the measured length may increase by 0.1".
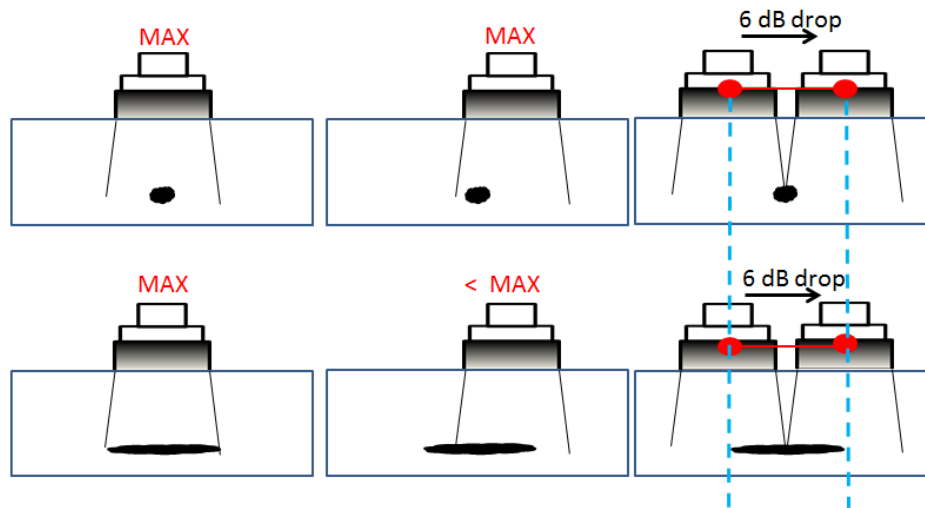
Figure 3-1: Diagram showing the overestimated length measurement of a small defect

Each of the LA1 slots was inspected at the end of Leg 1, at the bottom corner of the slot and on Leg 2, at the top corner of the slot. Both legs were inspected to determine the measured length and to compare the results to the actual slot size. Each slot was inspected on the second leg as well to determine the beam spread effect at longer wave path lengths.

A range of defect lengths were manufactured to better understand the beam spread effect on different defect lengths. For this procedure, B-Scans were created by moving the transducer along the length of each LA1 slot or hole. In order to determine the beam spread for each defect, B-Scans were taken along the length of the first and second leg of each slot.

3.1.3 Defect Orientation

The defect orientation test measured the reflected amplitude as the transducer was positioned at different angles relative to the defect as shown in

Figure 3-2. The measurements from this test indicate the angle at which the maximum amplitude will drop by 6 dB. The maximum amplitude measured during the inspection occurs when the defect is oriented perpendicular to the transducer; however, defects located within steel welds are not always oriented parallel to the weld. This test will provide data that identifies the decrease in amplitude due to the defect orientation. The data can be used to identify an acceptable angle at which the defect can be inspected. The loss in amplitude due to the angle rotation can then be incorporated into the acceptance criteria.

This test evaluates three slots from the LA1 plate to determine the effect the defect angle has on different sized defects. As discussed in Section 2.3.1, the reflected amplitude decreases depending on the defect angle and the defect size. The 3/8", 3/4" and 1.5" slots in the LA1 test specimen were inspected. These slots were inspected to determine the decrease in reflected amplitude as the transducer rotates about the defect for defects both larger and smaller than the transducer.
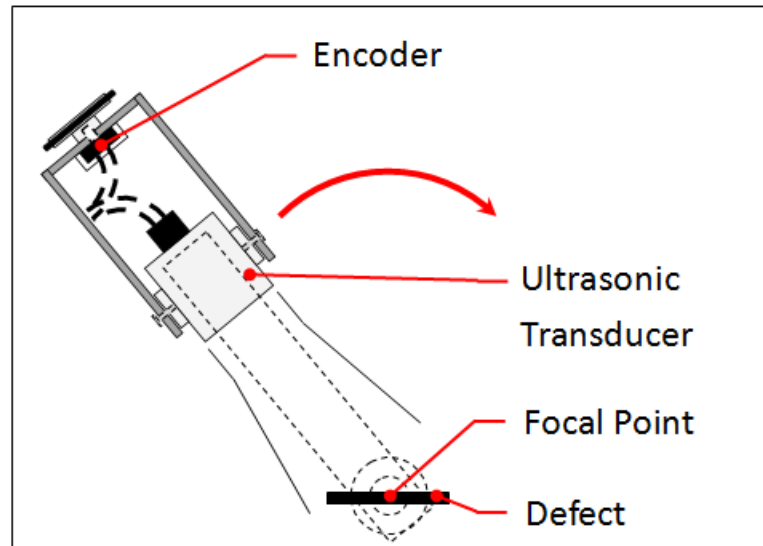
Figure 3-2: Defect Angle test setup

Figure 3-2 shows the test setup used to focus the acoustic wave on a single focal point throughout each inspection. This unique connection was used to maintain a constant distance from the defect while focusing the ultrasonic transducer to a focal point. This focal point was placed at the center of each defect to inspect each slot at the bottom of the first leg. As the transducer was positioned at different angles relative to the defect, an encoder attached to the transducer tracked its location. The rotation values were calculated from the encoder location points. Unique B-Scans were created using the rotation values calculated from the encoder location points. These B-Scans relate the amplitude reflected to the angle relative to the defect.

3.1.4 Transducer Rotation

The transducer rotation test evaluated the reflected amplitude as the transducer was turned about a focal point located at the center of the transducer

as shown in Figure 3-3. The AWS ultrasonic testing procedure allows the technicians to rotate the transducer by 10° during the initial scan to detect defects. As the technician initially scans the weld, the transducer is rotated slightly back and forth. Any indications with large reflected amplitudes are then thoroughly evaluated. This test looks to determine the amount of reflected amplitude received by the transducer as the wave is rotated away from the defect.

This test evaluated defect both larger and smaller than the transducer. The 1/4" and 1/8" flat-bottom holes in the FBH1 plate and the 3/8", 3/4" and 2.25" slots from the LA1 plate were inspected to determine the effect of transducer rotation on different sized defects. The flat bottom holes in the SDH1 and the bottom corners of each LA1 slot were inspected.
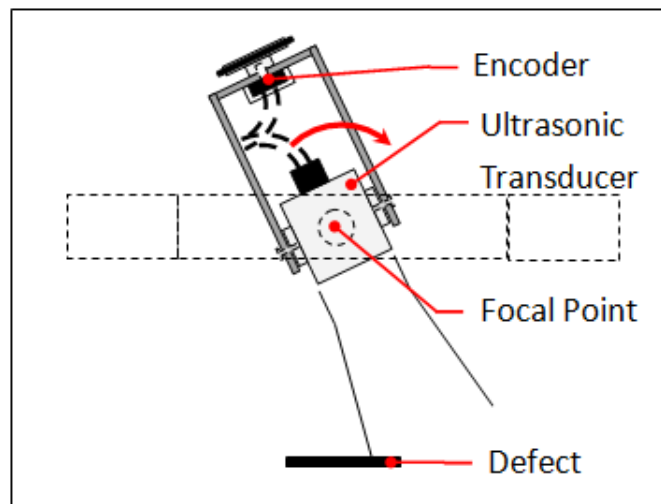
Figure 3-3: Transducer rotation test setup

In order to keep the transducer in the same location during rotation, a special connection, shown in Figure 3-3, was used. This connection was used to

42

maintain the same position as the transducer was turned. The transducer rotation tests require the acoustic wave to move on and off the defect. As the transducer was rotated, the encoder attached to the transducer tracked the location. The rotation values are then calculated from the encoder location points. B-Scans similar to the defect angle results were then created. These B-Scans relate the transducer rotation to a decrease in reflected amplitude.

3.1.5 Beam Spread

The beam spread tests evaluated the effect beam spread has on the length measurement. This test looks to identify the beam spread angle for slots both shorter and longer than the transducer.

The beam spread and the attenuation tests were conducted on the 1/16" diameter hole, the 3/8" slot, and the 3/4" slot in the LA1 plate. The 1/16" diameter hole, the 3/8" slot, and the 3/4" slot were chosen because the 1/16" and 3/8" slots are smaller than the transducer and the 3/4" slot is slightly larger than the transducer. B-Scans were developed to show the reflected amplitude relative to the transducer location. The B-Scans were initially conducted at a surface distance of 1.75" away from each slot. Each B-Scan was conducted after moving the transducer away from the slot at 1/4" increments to a maximum of a 6" surface distance. The B-Scans were then analyzed to identify the location at which the amplitude dropped to 50% maximum reflected amplitude. The 50% maximum amplitude locations are used to determine the measured length. The lengths are then compared to the wave path lengths at which to B-Scans were

taken. These tests look to determine if the measured lengths increase as the wave path length increases due to the defect size and the effect of beam spread.

3.1.6 Attenuation Factor

The attenuation tests evaluated the reflected amplitude as the wave path length increases. As stated in Section 2.1.4, the wave energy is scattered and absorbed as the acoustic wave propagates through the material. The AWS ultrasonic testing code accounts for this energy loss by reducing the amplitude by 2 dB for every inch of wavelength. Other codes such as the ASME and API codes incorporate the DAC curve. This research looks to determine if the 2 dB assumption is appropriate.

The data for the attenuation tests were collected from the beam spread tests' B-Scans. The maximum reflected amplitude from each B-Scan was recorded and compared to the inspection distance. The top and bottom corners of each LA1 slot reflect the amplitude peaks; however, these amplitudes are not similar due to the attenuation effect. These corners provide ideal attenuation measurements because they are similar in geometry and were inspected at different wave path lengths.

An additional test was performed to evaluate the effect of attenuation. This test evaluated the large horizontal pattern on the Side 7 of the SR1 plate at multiple distances to generate results similar to a Distance Amplitude Correction (DAC) curve. This test assumes that the roughness is constant throughout the wall area and that the roughness of the SR1 wall reflects constant amplitudes

over the wall area. This wall was chosen to replicate a defect that spans over the entire wall surface and can be evaluated at different wave path lengths. The decrease in reflected amplitude due to a attenuation at each wave path length is then compared to the 2 dB AWS assumption.

This test evaluated the SR1 plate with the horizontal pattern plate at multiple distances. In order to avoid the near field interference, the transducer was placed a distance of 1.5" away from the side. The transducer is then moved back 1/4" until a distance of 4" is attained. A-Scans are taken at each distance and the wall reflection is recorded. These reflections are then organized to generate results comparing the measured reflected amplitude to the wave path length at the time of inspection.

Most DAC curves in the ASME and API only evaluate 3 to 4 defects to establish a curve; this test evaluates 13 locations with different wave path lengths. By including more locations, a curve would not have to be assumed. These locations should identify the reflected amplitude from the same defect at different wave path lengths. Multiple reflections should provide a better representation of the attenuation for the entire waveform.

3.1.7 Wedge Angle

The two wedge angle tests compared the change in reflected amplitudes between the 45°, 60° and 70° AWS angle beam probes when evaluating similar defects. As discussed in Section 2.5.1, the AWS code assumes that each defect

is oriented vertically. The AWS code adjusts the acceptable reflected amplitude value in the acceptance criteria to account for the wedge angle.

The AWS ultrasonic testing acceptance criterion considers the probe angle relative to a vertical defect. The AWS assumes each defect is oriented vertically within the weld. The 90° horizontal beam shown in Table 4 refers to a horizontal beam traveling at an incidence angle of 90° and inspecting a vertical flaw at a perpendicular angle. The AWS assumes that the 90° orientation achieves the greatest reflected amplitude and that no adjustments need to be made in the acceptance criteria. Table 4 shows the adjustments made to the acceptable reflected amplitude based on each angle. As the angle of incidence decreases, the beam inspects the defect less efficiently resulting in lower reflected amplitudes. The adjustments to the acceptance criteria compensate for the amplitude loss by increasing the required sensitivity used to detect the defect. A defect inspected at 45° requires a reflection 11 dB more sensitive than a defect inspected at a 90° angle.

Table 4: Adjustments made to the acceptance criterion based on transducer angle

Angle of Incidence	Amplitude Change (dB)
90° (horizontal beam)	**0**
70°	**6**
60°	**9**
45°	**11**

The first attenuation test evaluated the large horizontal pattern on Side 7 of the SR1 plate to replicate the wedge angle effect on a vertical crack. Each angled probe inspected the same 1.25" deep region on wall. In order to inspect the same depth, each transducer had to be moved to the appropriate distance

46

away from the wall which changed the wave path length. The results accounted for the attenuation effect caused by the change in wave path length by incorporating the 2 dB drop used in the AWS code. Each inspection yielded an A-Scan containing the reflected amplitude from Side 7 of the SR1 plate. These amplitudes were then compared to the wave's incident angle to determine if the AWS assumptions are valid.

An additional test was conducted to identify the change in reflected amplitude due to a change in defect orientation within the weld. This test evaluates the reflected amplitude from several slot corners of different lengths. The AWS acceptance criterion assumes any indication is oriented vertically; however, not all defects are aligned vertically. This test looks to identify the effectiveness of each transducer in inspecting multiple corners and compare them to the AWS assumptions.

The second attenuation test inspected the bottom corner of the 1/16" diameter hole, the 3/8" slot, and the 3/4" slot in the LA1 plate using all three angle beam transducers. Due to the variation between transducers, the SC block described in Section 3.4.30 was used to calibrate each transducer. A-Scans of the maximum reflected amplitude for the bottom corner of each defect were created. The reflected amplitudes were then compared using the calibration data to determine if the AWS acceptance code adjustments are effective.

3.1.8 Defect Sizing

The defect sizing test evaluated manufactured defects within steel welds using the AWS sizing procedure. Instead of evaluating steel specimens with fabricated slots, this test sizes realistic defects using the 50% amplitude drop similar to the AWS ultrasonic procedure. The effectiveness of the AWS sizing technique can be more accurately evaluated by inspecting realistic defects in fabricated welds.

The SMB-11 plate contains three fabricated defects located in its weld. Each defect was inspected on both faces, on both sides because the AWS code requires each weld to be inspected from multiple sides if possible. The root crack (Defect 3) was inspected on both the first and second leg of the wave path due to its location at the bottom of the weld. This provides a great example of the beam spread effect on the length measurement.

As stated in Section 2.1.1, not all surfaces are available during bridge inspections. This test inspects every defect from every angle and compares the length measurements.   B-Scans were developed to determine the length measurement for each defect. After the defect was identified, the transducer was oriented perpendicular to the weld and moved parallel to the weld. The reflected amplitude was evaluated to determine the 6 dB drop location associated with the edge of the defect.

3.2 A-Scans and B-Scans

This section describes the A-Scan and B-Scan data acquisition used in each test. The ultrasonic waves received by the transducer are displayed in an A-Scan shown in Figure 3-4. The A-Scan displays the received amplitude in millivolts vs the time that the reflected amplitude was received. Defects identified in an A-Scan can be located by calculating the position using the reflection time, material properties and the ultrasonic transducer angle.

B-Scans relate the reflected amplitude of an A-Scan time range to a location as seen in Figure 3-5. In order to associate a location to each A-Scan, the encoder described in Section 3.3.2 was attached to the transducer. Each time range used to evaluate the defect is calculated using the transducer angle, plate material properties and the plate's geometry to locate the desired indication.

Figure 3-4 and Figure 3-5 shows an example of both A-Scans and B-Scans of the same test. The two vertical lines in Figure 3-4 represent the time range calculated to analyze the defect indication. The maximum amplitude from each time segment is identified and associated to its location provided by the encoder. The B-Scan displays the maximum amplitudes found in the given time range versus the encoder locations as seen in Figure 3-5.
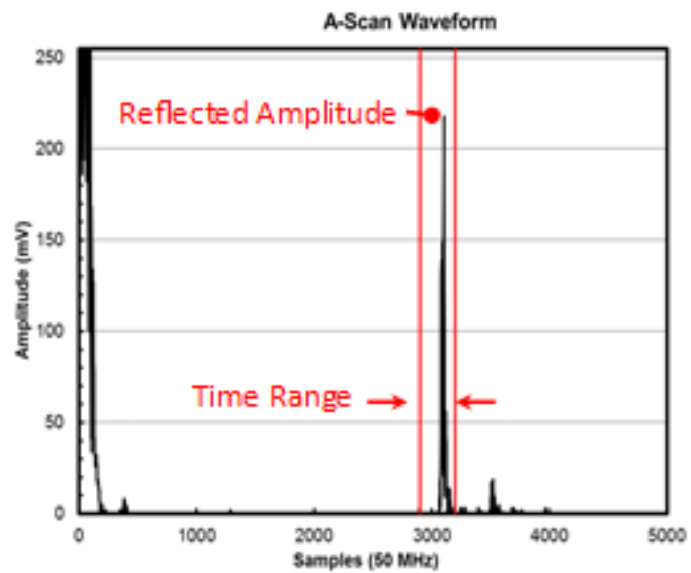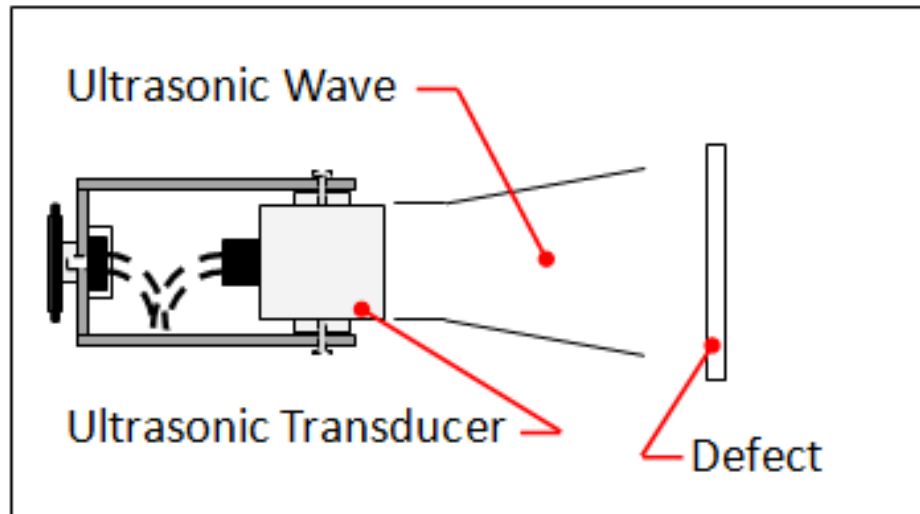
Figure 3-4: A-Scan waveform example indicating the B-Scan time range
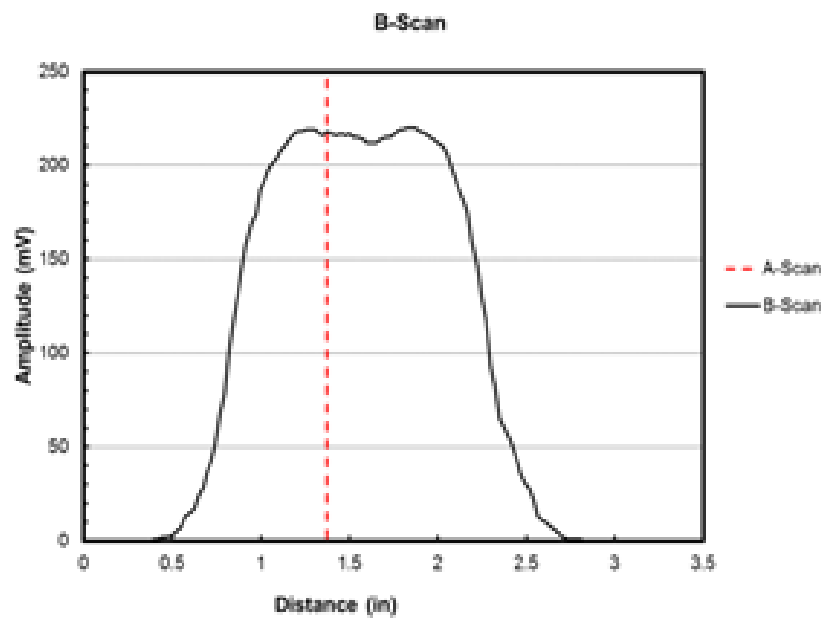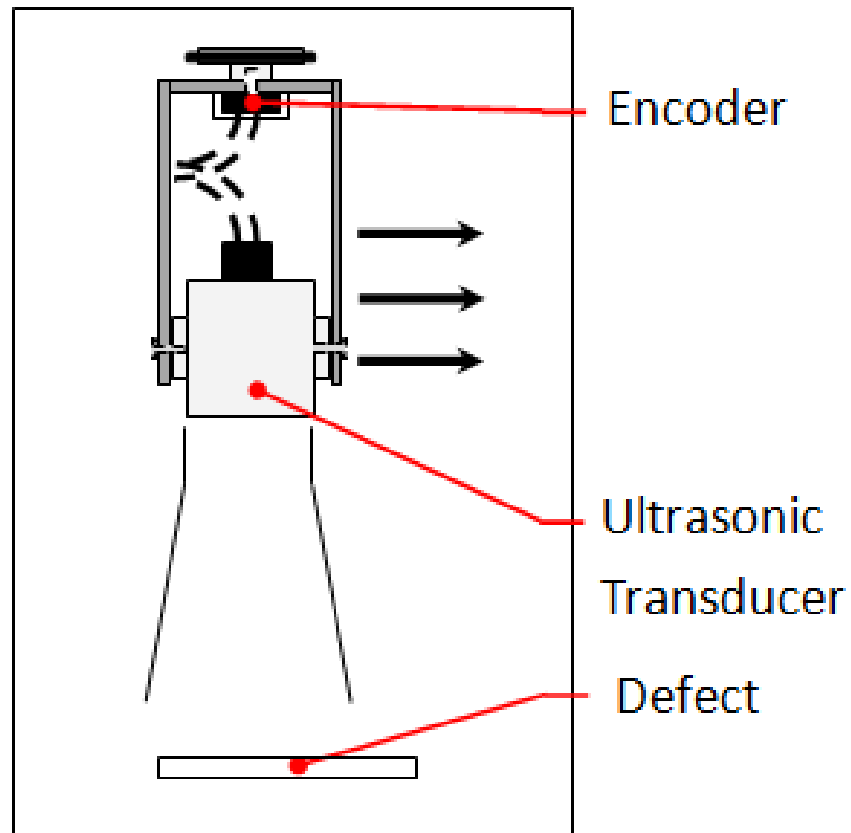
Figure 3-5: B-Scan showing location of the A-Scan measurement

3.3 Test Setup and Equipment

The experimental test apparatus used in each test procedure accomplished for this research is shown in Figure 3-6. The test apparatus consisted of an ultrasonic transducer, encoder and a pulser-receiver controlled by a LabView program on a laptop. The three AWS ultrasonic transducers with acrylic wedges were the 45°, 60° and 70° probes. The USB-UT350 pulser-receiver was chosen for its encoder capabilities. The S1 encoder was chosen for its size and axel location.
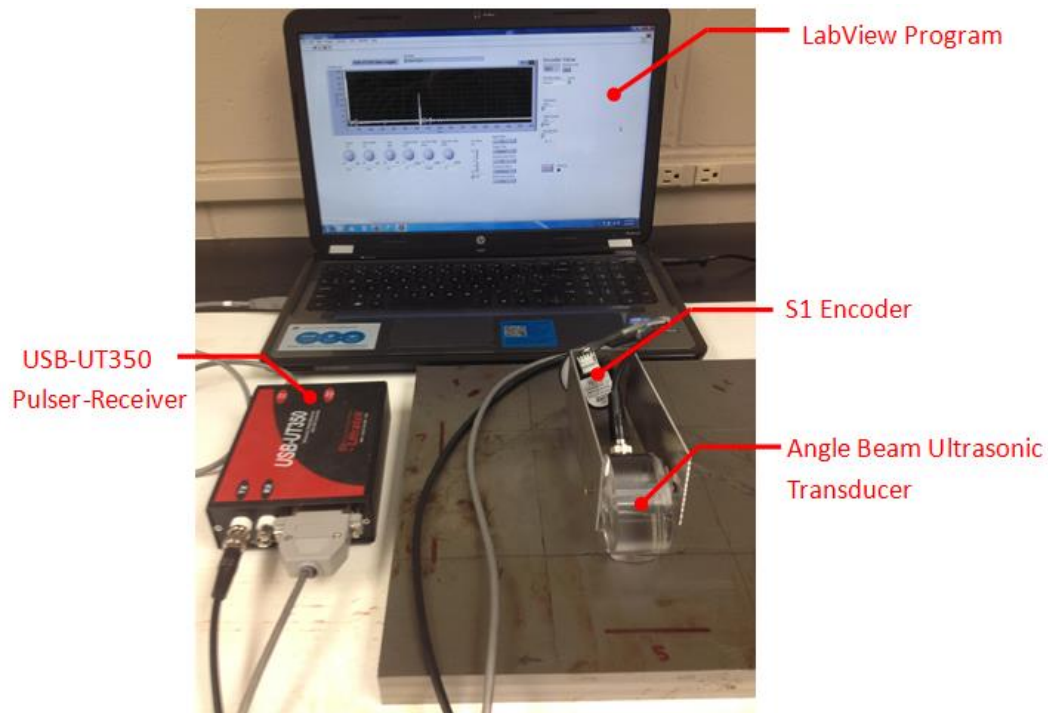
Figure 3-6: Experimental Setup

Figure 3-6 shows the basic setup for the test procedures. The LabView program controls the USB-UT350 pulser-receiver, and the pulser-receiver uses the transducer and encoder to collect data to display on the LabView program. The pulser-receiver receives the signal from the Labview program to send

electric pulses to the ultrasonic transducer. When the piezoelectric crystals in the ultrasonic transducer are charged, the material expands generating an acoustic wave. The reflected acoustic wave compresses the piezoelectric crystal sending a voltage to the pulser-receiver. The reflection time and reflected amplitude are recorded. The recorded information is then sent from the pulser-receiver to the LabView program and displayed on the screen.

Figure 3-6 shows the USB-UT350 connections to both the transducer and the encoder. An L-com connection cable, measuring 3 feet connected the transducer to the RX port on USB-UT350 pulser receiver. A pin connection cable, measuring in 3 feet, connected the S1 encoder 5 pin connection to the USB-UT350 25 pin connection.

3.3.1 Ultrasonic Transducers

The research used a standard AWS ultrasonic transducer to generate and receive acoustic waves at a frequency of 2.25 MHz. The transducer contains a square 0.625" x 0.625" piezoelectric crystal. The AWS ultrasonic transducer was designed to attach to the 45°, 60° and 70° acrylic wedges that angle the wave. A coating of motor oil was placed between the transducer surface and the wedge to transfer the acoustic waves from the transducer to the acrylic material. During each UT scan a coating of Sonotech UT-X couplant was applied to the surface of the steel specimens to transmit the shear waves.

3.3.2 Encoder, Contact Wheel and Connection

The research used an S1 encoder during the test measurements to associate the A-Scan waveforms to locations along the movement path. A contact wheel was secured to the encoder axel with a set screw. The encoder increases by 2880 units per rotation, or 8 units per wheel degree. As the encoder values increase, the encoder sends information to the USB-UT350, and at the same time, the USB-UT350 saves both the encoder location and ultrasonic waveform data. These data were sent to the LabView program and are saved to an excel file for analysis.

An aluminum frame was used to connect the 70° angle beam wedge transducer to the encoder as seen in Figure 3-6. Two 1/2" x 1/2" x 5/8" acrylic sections were glued to the sides of the 70° angle beam wedge and were used as drill locations for the encoder frame connection. Two screws attached the encoder to a 1/16" thick aluminum frame. The encoder was attached to the aluminum frame using a nut and gripping washer.

3.3.3 LabView Program and Data Acquisition

A LabView program was designed for the USB-UT350 pulser-receiver to acquire ultrasonic testing waveforms as well as encoder measurement information. This program controlled all parameters including gain, pulse width, encoder measurements and wave path display length. A Standard Scope program was provided by the USB-UT350 manufacturer, but the program was unable to automatically acquire A-Scans associated with an encoder location.

54

The customized LabView program was capable of automatically acquiring the A-Scan data with its associated encoder location and was used in every test procedure.

3.4 Test Specimens

The test materials used as a part of the research consisted of several steel specimens with varying thicknesses and unique machined features. Each specimen was designed with unique characteristics for the procedures described in Section 3.1.

3.4.1 FBH1

The FBH1 is a 7" x 7" x 3/4" square A36, steel plate containing four 1/2" deep holes of varying diameter shown in Figure 3-7. The plate has four side drilled holes drilled of 1/4", 1/8", 1/16", 1/32" diameters drilled 1/2" into the plate. The size of the 1/32" hole was on the limit of detection because it is close to half the wavelength of a 2.25 MHz transducer. The other defects have diameters 2, 4 and 8 times the size of the 1/32" hole. Schematics of the FBH1 plate shown in Figure 3-7 are located in Figure A-1.
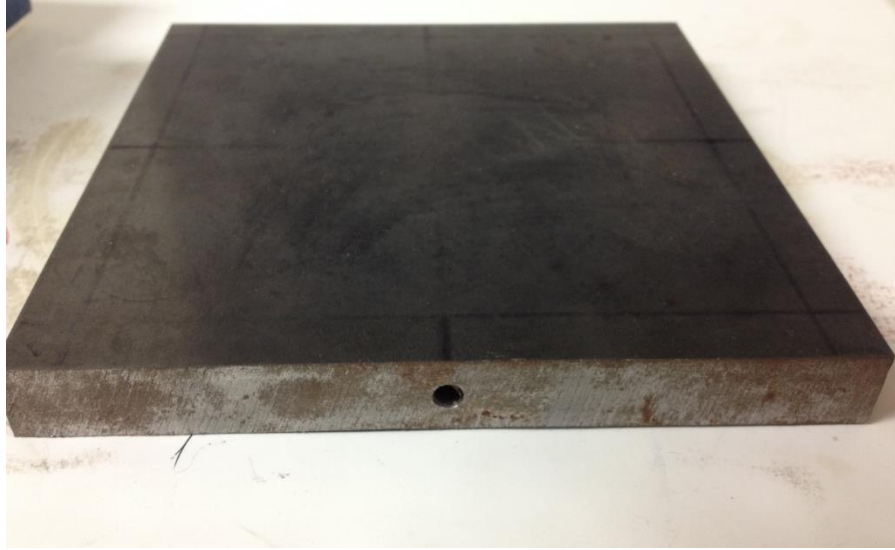
Figure 3-7: FBH1 Plate containing four 1/2" deep flat bottom holes

3.4.2 LA1

The LA1 specimen is made of A36 steel, 1" thick 12"x12" with electric discharge machined (EDM) cuts. There are eight cuts of varying lengths, as seen in Figure 3-8. Four rectangular slots were cut through the steel at different lengths. Three fingernail-like grooves were made in the steel to resemble fatigue cracks. One 1/16" diameter hole, similar to the 1/16" diameter hole used for calibration, was cut into the plate. The defect lengths were designed so that some defect lengths were smaller than the transducer and some defect lengths were larger than the transducer. Schematics of the LA1 plate shown in Figure 3-8 are located in Figure A-3.
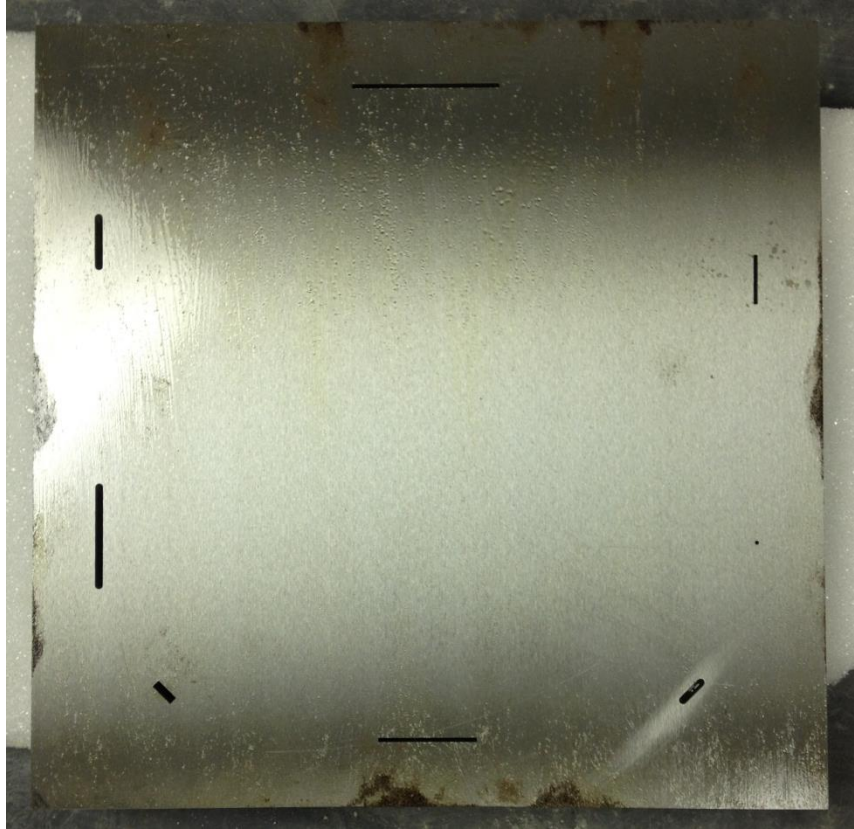
Figure 3-8: LA1 test specimen containing 8 defects with different geometries

3.4.1 SR1

The SR1 specimen is an 8" x 8", 2" thick, A36 steel plate machine cut into an octagon to expose eight sides with different surface finishes and patterns. The specimen's surface finish includes: three sides with cross-hatched finishes of different groove finishes, three sides with horizontal finishes of different groove finishes, one side with two large grooves cut via grinder to form a horizontal and vertical defect, and one side with the smallest possible fabricated roughness. These surfaces are pictured in Figure A-4 to Figure A-10.   In order to quantify the roughness of each side, a profilometer was used to scan each surface and determine the largest measured roughness as shown in Table 5.

Table 5: Surface roughness of SR1 plate sides

	Pattern	Roughness
Side 1	Machine Finish	324
Side 2	Finest Finish	68
Side 3	Large Profile Finish	1112
Side 4	Medium Profile Finish	600
Side 5	Small Profile Finish	165
Side 6	Large Horizontal Finish	1161
Side 7	Small Horizontal Finish	541
Side 8	Grinder	-

The fatigue specimens loaned to this research by Purdue University consisted of a steel frame which was fatigued to failure as seen in Figure A-11 to Figure A-17.   Each fatigue surface was scanned using the profilometer to determine the maximum surface roughness as shown in Table 5.   Side 4's roughness was larger than the profilometer's maximum measureable roughness, 2000 µin. The reflected amplitudes from each surface with fatigue failure were then compared to the amplitudes from the SR1 surface finishes.

Table 6: Surface Roughness of Fatigue Specimen sides

	Roughness
Side 1	600
Side 2	875
Side 3	718
Side 4	2000*
Side 5	377
Side 6	330

3.4.2 SMB 11

The fifth specimen was a 12" x 17" x 1.25", A36, welded steel plate obtained from the performance testing of the Sherman-Minton Bridge.   The

welded plate, as seen in Figure 3-9 has three fabricated cracks implanted into the volume of the weld. These implanted defects provided a realistic sample of cracks in steel welds. Schematics of the SMB-11 plate shown in Figure 3-9 are located in Figure A-2.
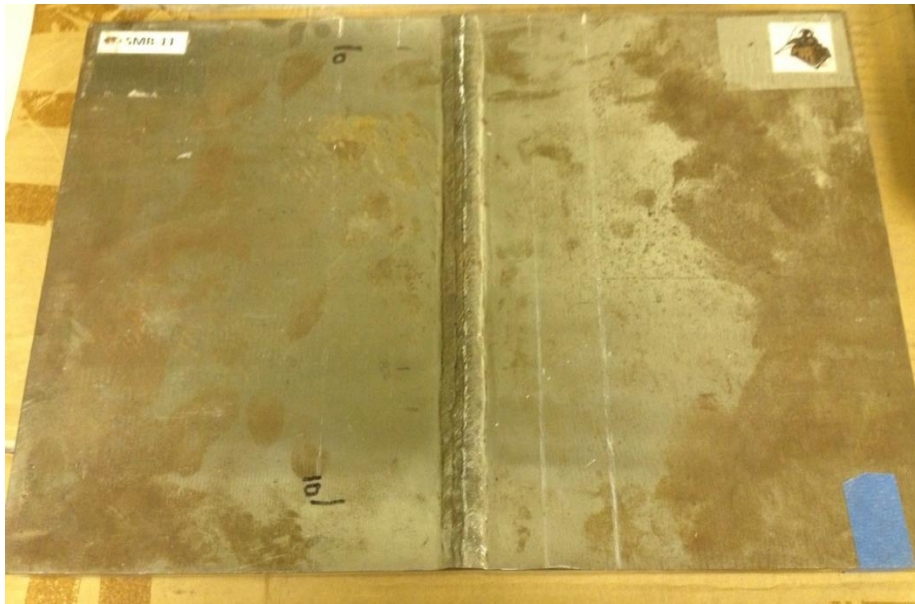
Figure 3-9: SMB-11 plate

3.4.3 Sensitivity Calibration Block

The AWS D1.5 code requires the ultrasonic equipment to be calibrated prior to each examination. The Sensitivity Calibration (SC) Block was used to calibrate the transducers used in this research. The calibration procedure referenced in Annex F of the AWS D1.5 states:

"**FA2.4.2** *The transducer shall be set on the SC block in position:*

N for 70° angle

O for 45° angle

P for 60° angle

The maximized signal from the 1.6 mm (1/16 in) hole shall be adjusted to attain a

horizontal reference-line height indication."

The SC calibration block has two 1/16 in diameter holes located within the material as seen in Figure 3-10. The SC Block was designed so that the acoustic waves of each angled transducers travel 1" into the material to detect each hole from the designated positioning.
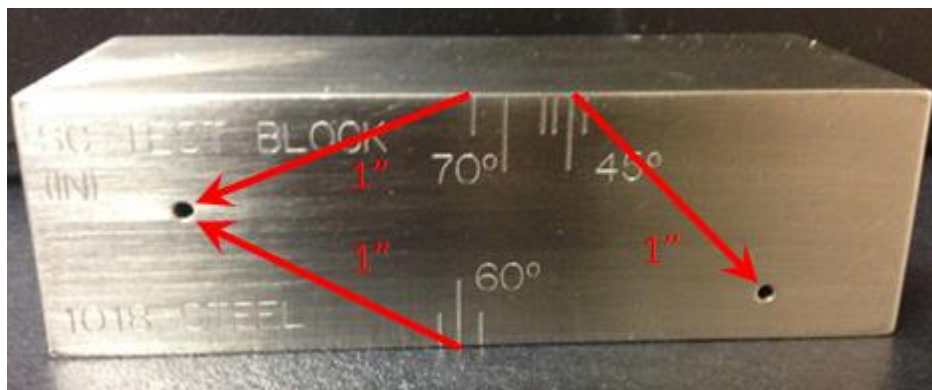
Figure 3-10: Sensitivity Calibration Block

4 RESULTS

This chapter contains the results of the ultrasonic testing conducted to identify and quantify the various factors that impact ultrasonic test measurements. Section 4.1 presents the results from all the test procedures described in Chapter 3. Section 4.2 describes the use of PAUT to demonstrate the technology's S-Scan capabilities.

4.1 Ultrasonic Testing

4.1.1 Length Measurement

The length measurement test determined the effectiveness of the 6dB drop technique described in the AWS procedure to size defects. The length procedure described in Section 3.1.2 was used to develop B-Scans to measure the length of each defect in the LA1 plate. B-Scans were created to evaluate all 8 EDM slots within the LA1 plate. In order to determine the beam spread effect on the measured length, each defect was measured on the first leg and then again on the second leg. The length measurements are compared to the actual defect length in Figure 4-1 and Figure 4-2. The length measurements in both figures are organized by the leg at which the defects were inspected.

Table 7: The LA1 defect length measurements

Slot Length	Slot Type	Leg 1		Leg 2	
		Average Length (in)	Length (%)	Average Length (in)	Length (%)
0.0625	Hole	0.26	412	0.29	458
0.375	Fingernail	0.43	116	0.60	160
0.375	Slot	0.39	104	0.60	159
0.75	Fingernail	0.60	80	0.63	83
0.75	Slot	0.74	99	0.67	89
1.5	Fingernail	1.51	100	1.43	95
1.5	Slot	1.48	99	1.40	93
2.25	Slot	2.20	98	2.19	97

The data shown in Figure 4-1, Figure 4-2 and

Table 7 indicate that the length measurements are impacted by the defect length relative to the transducer length. Defects shorter than the 0.625" transducer length were affected by the beam spread and were initially oversized. Table 7 shows that the length measurements of the 1/16" and 3/8" slots increased from 0.257" to 0.286" and 0.391" to 0.5975", or 11% and 53%, respectively. Defects larger than the transducer length were measured near or shorter than the defect.
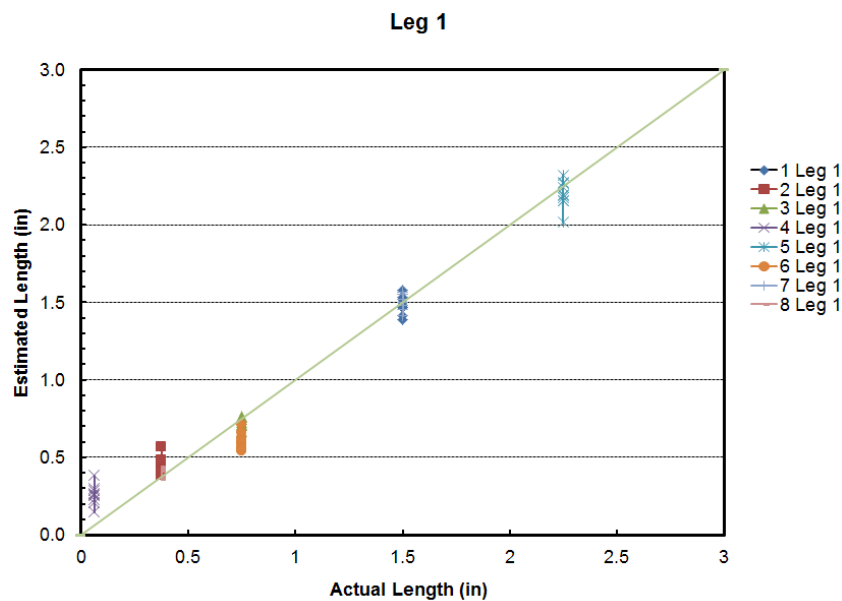
Figure 4-1: Length measurements vs actual length of all LA1 defects in Leg 1

The data in Table 7 indicate that defects with larger volumes are more accurately measured. The 0.75" fingernail slot measured 0.15" shorter from both legs than the actual defect length due to the fingernail geometry of the groove. The fingernail slot represents the geometry of a fatigue crack where the length value is twice the depth value and is smaller in geometry than the slot of the

63

same length. The loss in defect volume, caused the measured length to be undersized.
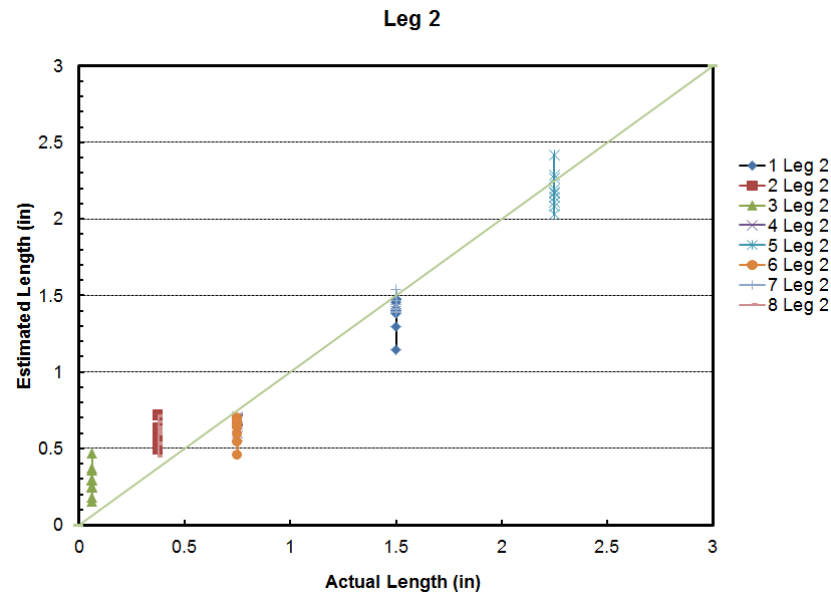
Figure 4-2: Length measurements vs actual length of all LA1 defects in Leg 2

The results in Table 7 show that the slots smaller than the transducer are typically oversized, while measurements of slots equal or larger than the transducer can be accurately sized or slightly undersized. In order to better understand the beam spread effect on defects smaller than the transducer, the slots shorter than the transducer were further evaluated in the beam spread test measurements.

4.1.2 Beam Spread

The beam spread test further investigated the impact of beam spread on sizing defects longer and shorter than the transducer length. A series of length measurements were conducted on the 1/16" diameter hole, 3/8" slot, and the 3/4" slot in the LA1 plate. These defects were chosen because the 1/16" hole and the

3/8" slot were shorter than the 0.625" transducer length, and the 3/4" slot was longer than the transducer length. Similar to the length measurement tests, the measured defect edges were associated with a 6 dB drop in maximum reflected amplitude.

During this test, the transducer was placed on the steel specimen's surface at various surface distances away from the defect. Due to the near field interference calculated at 1.4 inches, the defect was initially inspected at a wave path length of 1.86" or a surface distance of 1.75" away. The wave path lengths are identified in Figure 4-3, Figure 4-4 and Figure 4-5. This process was repeated while moving the transducer away from the defect by 0.25" increments until a 6" surface distance was attained. Figure 4-3 to Figure 4-5 show two data point groups that represent the left and right measured edges of each length measurement. The thin slanted lines are trend lines representing the slope of each group of data points, and the thick slanted lines represent the calculated beam spread angle of the transducer.
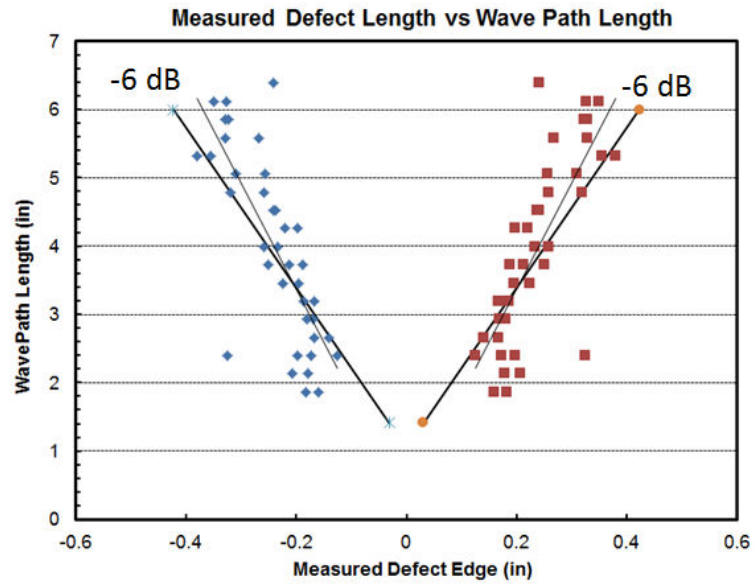
Figure 4-3: Beam spread test results of 1/16" diameter hole in LA1 plate
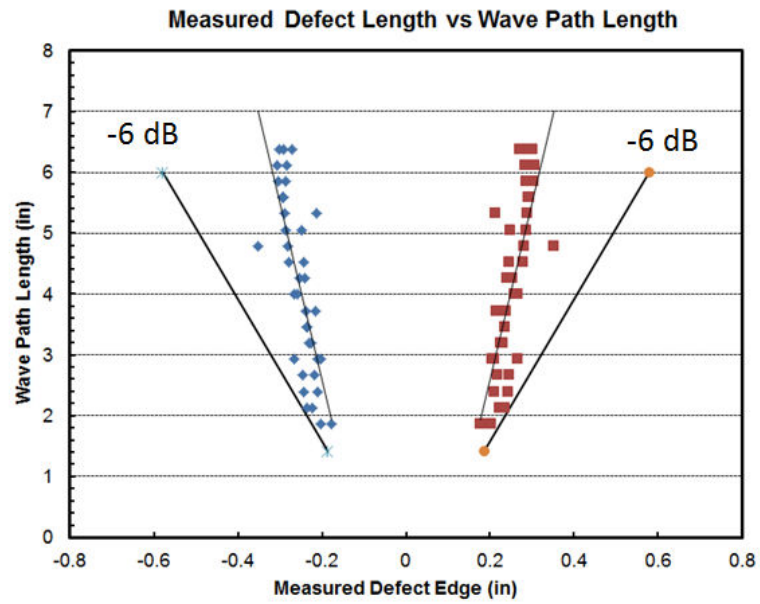
Figure 4-4: Beam spread test results of 3/8" slot in LA1 plate

66
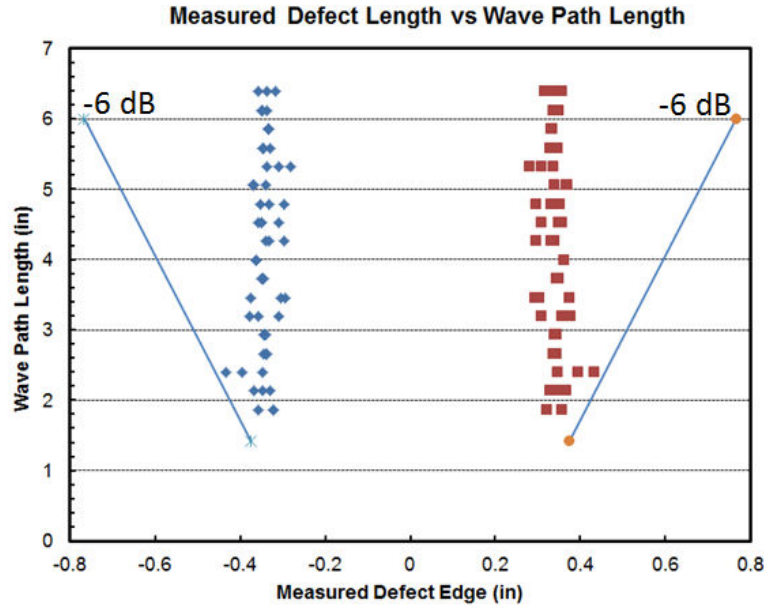
Figure 4-5: Beam spread test results of 3/4" slot in LA1 plate

The defect's maximum reflected amplitude was identified in each B-Scan to determine the 6 dB drop associated with both defect edges. Figure 4-3 to Figure 4-5 show the measured lengths versus the calculated wave path distance. The thick slanted lines represent the angle of dispersion, γ, calculated using Equation 2.1.2-3. The wavelength was calculated at 0.0569" based on the 0.128 in/μs shear velocity of the steel plate and the 2.25 Mz frequency at which the transducer operates. The length of the piezoelectric transducer, A, was 0.625", and the constant k_{dB} found on Table 2 in Chapter 2, was 0.44 based on the desired -6dB drop in the echo field. The angle of dispersion was calculated at 4.594°. The data shown in Table 8 indicate that the length measurements are impacted by the defect size as well as the wave path length. As seen in Figure 4-3 to Figure 4-5, the beam spread, α, affects the length measurement of defects smaller than the transducer as the wave path length increases.

The measured beam spread angles in Table 8 were calculated using the average initial measured length and the average maximum measured length. The differences from the maximum and initial measured lengths were used along with the difference in wave path length of 4.52" from the initial inspection to the farthest inspection. The results found in Table 8 indicate that the beam spread angle greatly impacts the length measurement of defects smaller than the transducer.

Table 8: Beam Spread Angle test results

Slot Length	Average Initial Measured Length	Average Maximum Measured Length	Measured Beam Spread Angle (°)
1/16"	0.34"	0.68"	4.79
3/8"	0.38"	0.59"	3.00
3/4"	0.67"	0.69"	0.29

The initial length measurements were controlled by the larger of either the transducer length or the defect length. As shown in Table 8, the ultrasonic measurement of the 1/16" slot length measurement at a wave path length of 1.81" indicated an average length of 0.34", or 545% of the actual defect length. The 3/8" slot's initial measurement revealed the average length measurement was 0.38", or 102% of the actual defect length. The length measurements of defects smaller than the transducer are only 0.04" different in length, and approximately 57.8% (or slightly over half) of the transducer length. However, the 3/4" slot initial length measurement found that the average length measurement was slightly undersized at 0.668", or 89% of the defect length.

The effect of the beam spread is related to the size of the defect. Smaller defects are impacted greater by beam spread at longer wave path lengths. The average initial length measurements and maximum length measurements of the 1/16" hole are 0.3407 inches and 0.6757", respectively. The 1/16" defect yielded a 98% increase in measured length when evaluated from a longer wave path length. The average initial length measurements and maximum length measurements of the 3/8" slot are 0.38" and 0.59", respectively. The 3/8" defect saw a 55% increase in measured length when evaluated at a further distance from the defect. The average initial length measurements and maximum length measurements of the 3/4" slot are 0.668" and 0.6885", respectively. The 3/4" defect only yielded a 3.1% increase in measured length.

Length measurements for defects smaller than the transducer length are inaccurate due to their echo field behaviors. The maximum reflected amplitude from the larger slots drops more severely as the acoustic wave moves off the defect. The large slot reflects a larger portion of the acoustic wave at the maximum reflected amplitude. As the transducer is moved off the slot, the reflected amplitude drops significantly, resulting in more accurate length measurements. Smaller slots reflect a smaller portion of the acoustic wave at the maximum reflected amplitude. As the defect is moved off the small slot, the reflected amplitude drops more gradually which results in oversized length measurements.

4.1.3 Attenuation

The attenuation measurement test determines the decrease in reflected amplitude due to the attenuation of the material. This test analyzed the B-Scan amplitudes developed during beam spread angle test. As the transducer was moved away from the slot or hole, the reflected amplitude peaked at two locations: the bottom corner at the end of the first leg and the top corner at the end of the second leg. These corner traps, identified in Figure 4-6 to Figure 4-8, were analyzed because they consist of the same geometrical defect located at two different wave path lengths.

Table 9: Attenuation Test results

Slot Length	Average 1st Leg Amplitude	Average 2nd Leg Amplitude	Change in dB
1/16"	**220**	**87**	**-8.06**
3/8"	**253**	**120**	**-6.48**
3/4"	**236**	**126**	**-5.45**

The results in Table 9 indicate that the 2 dB drop with each wave path inch assumed by the AWS ultrasonic code is not accurate. The wave path length increases by 2.926" between the bottom and top corner measurements. This should result in a 4 dB drop in amplitude. According to Table 9, the average maximum reflected amplitude for the first leg of the 1/16" diameter hole was 220 mV. The measured amplitude found at 87 mV indicates an 8.06 dB change. As the defects' sizes grew, the change in reflected amplitude dropped. This means that a single attenuation value should not be used to characterize the loss in amplitude due to attenuation for all defects. The results in Table 9 indicate that

the attenuation effect on the reflected amplitudes is underestimated. It may be necessary to incorporate a DAC curve to improve the accuracy of the indication rating.
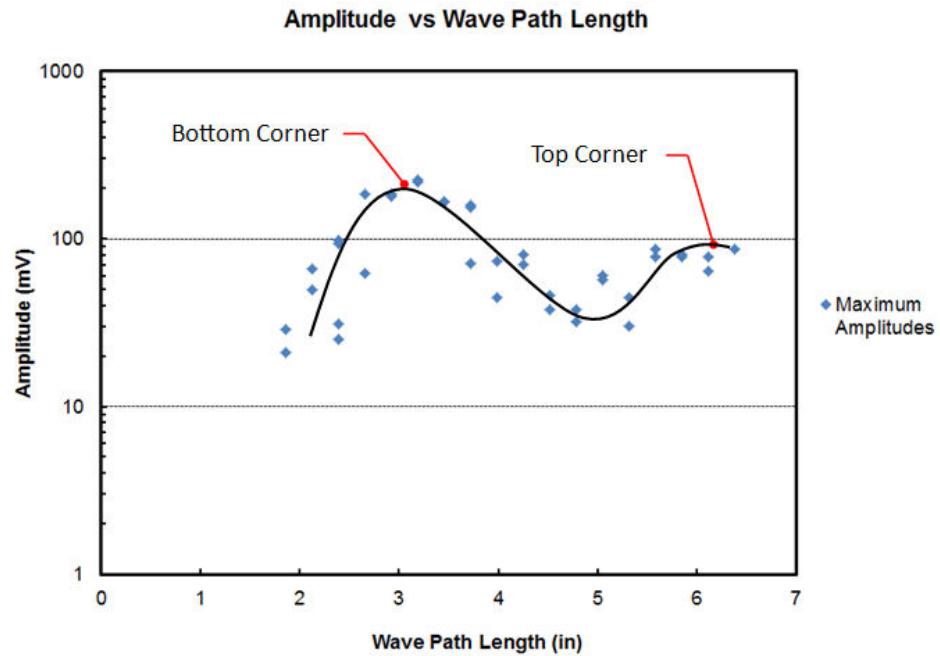
Figure 4-6: Attenuation of the 1/16" hole

71
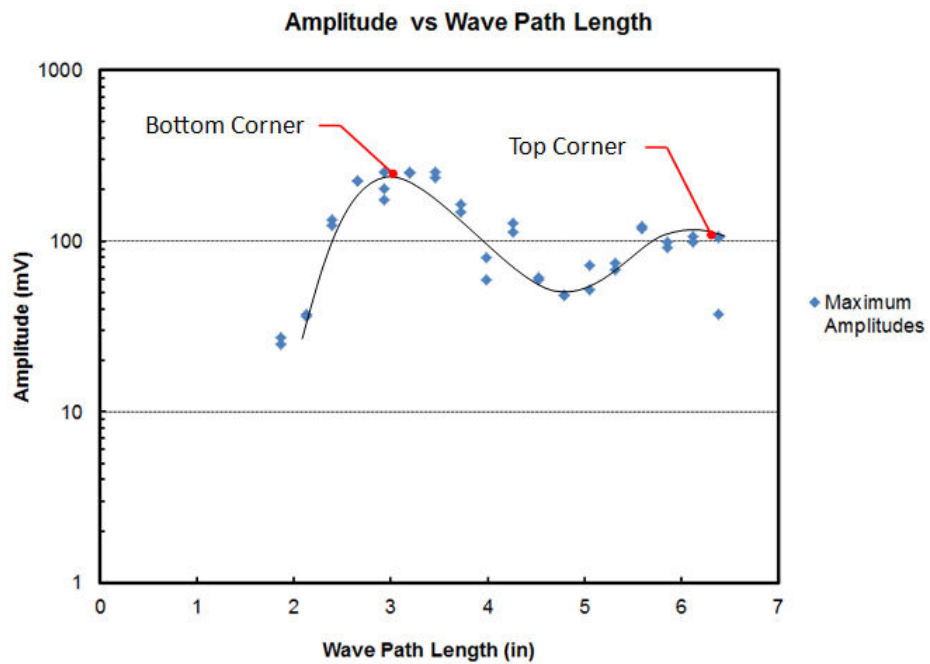
Figure 4-7: Attenuation of the 3/8" slot

Amplitude vs Distance
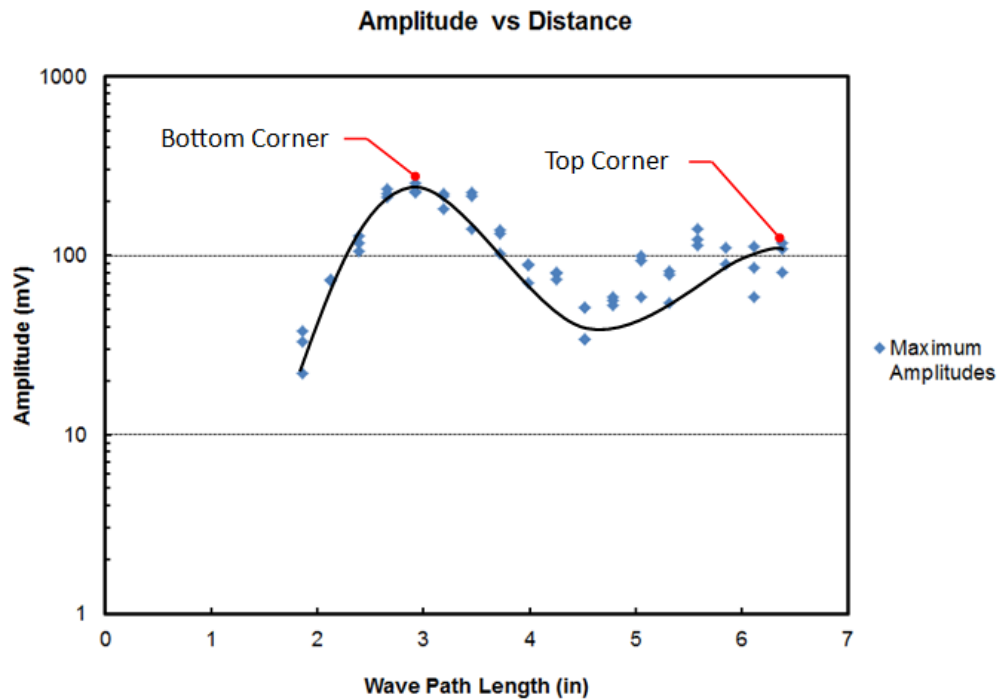
Figure 4-8: Attenuation of 3/4" slot

As described in Section 3.1.6, an additional test inspected Side 7 on the SR1 plate at multiple distances from the wall. The transducer was placed 1.5" away from the wall and moved away from the wall in 1/4" increments until a surface distance of 4" was attained. A-Scans were taken at each distance to determine the amplitude reflecting from SR1, Side 7. The results associated each maximum reflected amplitude to the wave path distance at inspection as seen in Figure 4-9 and Table 10.

The results shown in Figure 4-9 and Table 10 indicate that the reflected amplitude does not follow the 2dB decrease in amplitude. The results in Table 10 show the average reflected amplitude at the 2.93" wave path length is 104.6

mV, and the average reflected amplitude at 3.99" wave path length is 54,6mV. By using the AWS estimation, the reflected amplitude at the 3.99" wave path length should be 65.998 mV. Instead of the 2 dB/in drop assumed by the AWS, a 4 dB or 4.25 dB drop better characterizes the decrease in amplitude due to attenuation.

Table 10: SR1, Side 7 attenuation test results

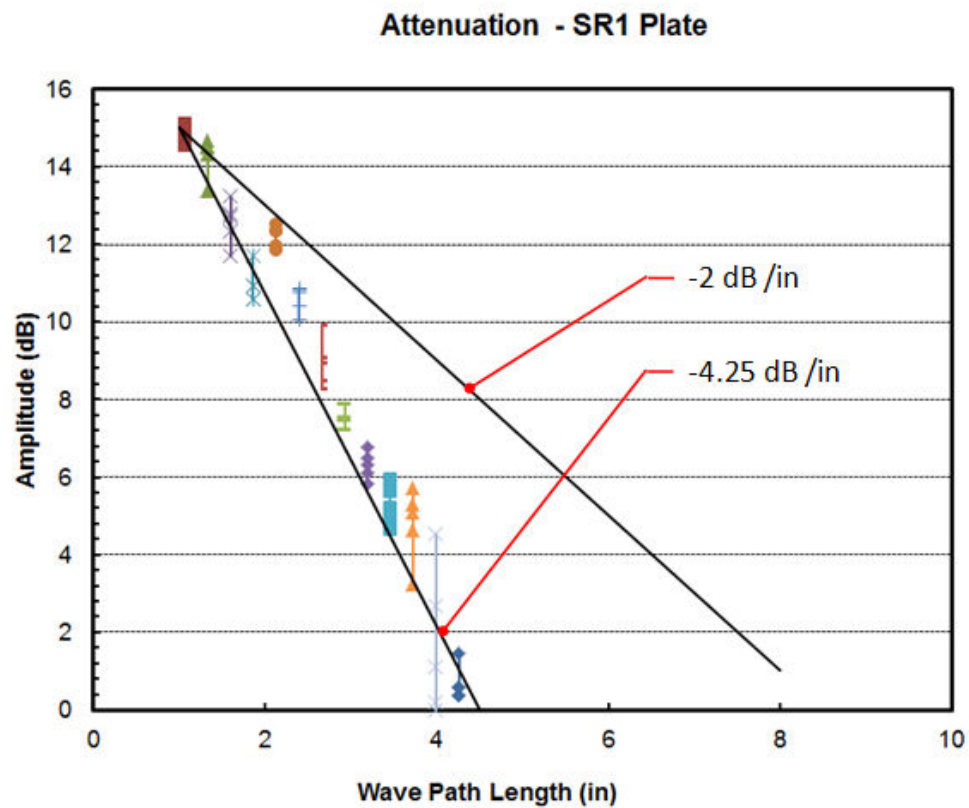| Wave Path Length Traveled	Surface Distance from Wall	Average Amplitude
1.06	1.00	244.2
1.33	1.25	228.2
1.60	1.50	187.0
1.86	1.75	155.4
2.13	2.00	179.2
2.39	2.25	149.0
2.66	2.50	123.4
2.93	2.75	104.6
3.19	3.00	91.0
3.46	3.25	80.8
3.72	3.50	76.8
3.99	3.75	54.6
4.26	4.00	47.6

Figure 4-9: SR1, Side 7 attenuation results

74

4.1.4 Defect Roughness

The defect roughness test determines the impact that defect texture has on the reflected amplitude. A series of tests were conducted to relate the change in reflected amplitude to the surface roughness of an edge or defect. The SR1 plate consists of seven sides with various surface finishes of different patterns and roughness. The reflected amplitudes from the SR1 walls were then compared to the reflected amplitudes from a specimen containing walls that were fatigued until failure.

Two different methods were incorporated in inspecting the SR1 and Fatigue specimens. B-Scans were created to evaluate a segment of each textured side of the SR1. These B-Scans were used to develop a profile of the reflected amplitude as the transducer inspected each side. The root mean square (RMS) value from each B-Scan was then calculated to better characterize each wall's profile. While B-Scans were the preferred method, the geometry of the fatigue specimen would not permit the use of the encoder. Instead, several A-Scans were captured at the location of the profilometer roughness measurements. Both top and bottom plate corners were present in the A-Scan waveforms due to the thinness of the fatigue specimens. The reflected amplitude due to surface roughness was assumed to be located between the two edge reflections. The reflected amplitudes from both test specimens are listed in Table 11 and Table 12.

Table 11: Manufactured specimen test results

Side	Pattern	Max	Average	Maximum	Minimum	Range

75

		Roughness (µin)	Amplitude (mV)	Reflected Amplitude	Reflected Amplitude	in dB
Side 1	Machine Cut	324	66.60	79	50	3.97
Side 2	Fine	68	36.90	43	32	2.57
Side 3	Large Profile	1112	45.10	55	30	5.26
Side 4	Medium Profile	600	43.78	49	37	2.44
Side 5	Small Profile	165	28.60	35	24	3.28
Side 6	Large Horizontal	1161	62.40	75	54	2.85
Side 7	Small Horizontal	541	75.50	98	55	5.02

Table 12: Fatigue specimen test results

Side	Max Roughness (µin)	Average Amplitude (mV)	Maximum Reflected Amplitude	Minimum Reflected Amplitude	Range in dB
Side 1	600	15.90	27	7	11.73
Side 2	875	23.00	31	11	9.00
Side 3	718	108.33	139	62	7.01
Side 4	2000	74.73	90	60	3.52
Side 5	377	116.55	159	70	7.13
Side 6	330	45.50	70	24	9.30

Table 11 and Table 12 indicate the amount of variability in each inspection associated with the high standard deviations in the reflected amplitudes. The range in dB was calculated using the maximum and minimum reflected amplitudes from each side. The results indicate a large discrepancy between the maximum and minimum amplitude values. Table 11 shows that the large profile pattern received amplitudes within a 5 dB range. Side 1 in Table 12 indicates measured reflected amplitudes almost 12 dB in range. These reflected amplitudes show trends associated with the wall texture, but also contain large amounts of variability. These results indicate that the reflected amplitude varies

due to the defect's texture, and that the AWS code may need to include these variations in their acceptance criteria.

Figure 4-10 and Figure 4-11 show the maximum reflected amplitude from each inspection vs the measured roughness. The data shown in Figure 4-10 indicates that the reflected amplitude was affected by the texture pattern as well as the texture roughness.
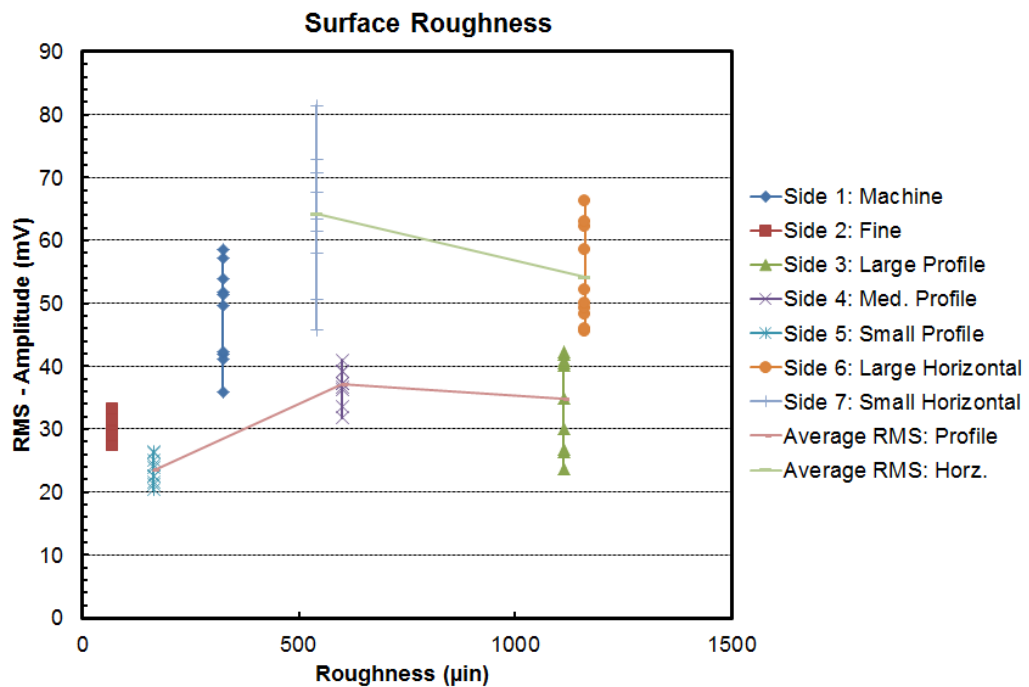
Figure 4-10: RMS values for each surface roughness B-Scan

The SR1 contained two sides that were designed to act as references: the fine finish and the manufacturer's cut finish. The fine finish side refers to the fabricated side containing the smallest roughness shown in Figure A-5. Figure A-10, in the appendix, shows a separate side that was left unaltered from its manufacturer's cut to replicate a typical steel surface encountered in the field. When the steel plate was purchased, the fabricator used a ban saw to cut the

steel plate. The course, jagged edges from the ban saw and the rusted portions caused by exposure combine to generate larger reflected amplitudes than the fine finish. The results in Table 11 show that the fine finish reflected a smaller average amplitude of 36.9 mV than the manufacturer's cut side which reflected 66.6 mV.

The horizontal finishes in the SR1 as seen in Figure A-8 and Figure A-9 consist of small ridges running along the inspected surface. These small grooves are oriented such that they impacted the reflected amplitude the most. The results in Figure 4-10 show that the horizontal finishes reflect the greatest amount of the acoustic wave back to the transducer. Table 11 shows that Side 7, containing the smallest roughness with a horizontal pattern, reflected the largest average reflected amplitude of 75.5 mV. Side 6, containing the largest roughness with a horizontal pattern, reflected lower reflected amplitude of 62.4 mV. The results indicate that acoustic waves reflected high amounts of noise resulting in high amplitudes at low wall texture roughness, the. As the roughness was increased and reached half the length of the transducer wavelength, the roughness impacted the acoustic wave path resulting in less of the reflected wave traveling back to the transducer.

The SR1 contained profile surface finishes as seen in Figure A-4, Figures A-6, and Figure A-7 consisting of semicircular grooves along the surface of the steel. The circular pattern scatters the reflection of the acoustic wave resulting in lower reflected amplitudes received by the UT transducer. The RMS values, shown in Figure 4-10, indicate that the low roughness profile finish reflected

small amounts of the acoustic wave. As the roughness increased, the interference of the reflected wave also increased. Once the roughness increased to half wavelength, the reflected amplitude decreased.
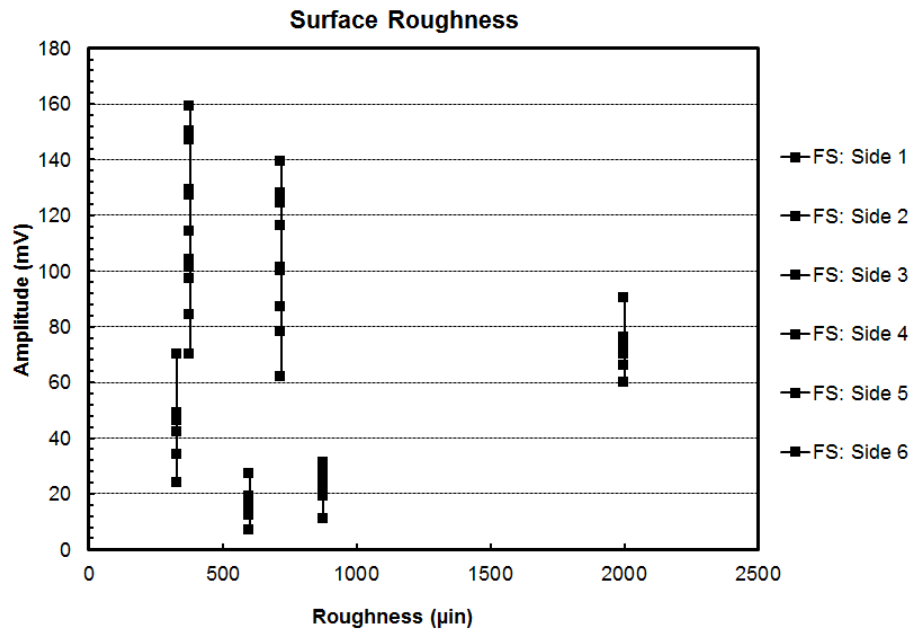
Surface Roughness

Figure 4-11: Maximum reflected amplitudes for each fatigue specimen side

In order to relate these surface roughness tests to real life conditions, two specimens containing edges fatigued to failure were inspected. These fatigue specimens are pictured in Figure A-11 to Figure A-17. B-Scans were unattainable due to the geometry of the weld. Instead, several A-Scan waveforms were taken at different locations on the specimen and used to characterize the roughness of the fatigued surfaces. The results shown in Table 12 indicate the reflected amplitude from the fatigue surfaces resemble the reflected amplitude from the horizontal finishes. As the surface roughness increases, the reflected amplitude decreases from excessive scattering. Figure 4-12 compares the average reflected amplitudes of the horizontal surface

79

textures and the fatigued specimens. The averages of both horizontal texture and fatigue crack walls increase in reflected amplitude as the roughness interferes with the reflected amplitude and decreases as the roughness interferes with the wave path reflection.
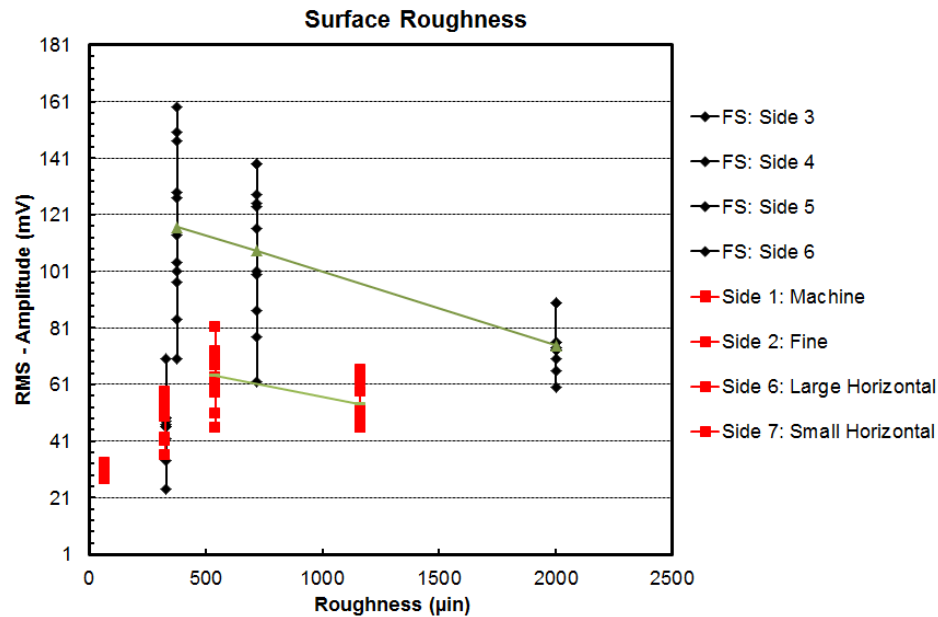
Figure 4-12: SR1 horizontal patterns results vs fatigued specimen results

4.1.5 Defect Orientation

The defect orientation test determined the decrease in reflected amplitude as the transducer rotated around a defect. Since the decrease in amplitude is affected by the defect size [14,15], the bottom corners of the 3/8" slot, 3/4" slot and the 1.5" slot were inspected. As described in Section 3.1.3, the transducer was rotated about a focal point, which allowed the transducer to inspect the same location on the slot at multiple angles. This focal point was located on the

edge of each slot to allow the transducer to inspect the defect's bottom corner. The bottom corner was located at the end of the first leg of the wave path.

Each inspection angle was tracked by the encoder to produce unique B-Scans. The encoder tracks the location as the transducer rotates about the focal point. The inspection angles can be then calculated using the wheel diameter, distance from the encoder to the focal point and the encoder location points. The B-Scans were then analyzed to identify the angle at which the maximum amplitude dropped by 50%. The 50% drop in maximum amplitude was identified in order to compare the rate of decreasing amplitude due to the defects size. Figure 4-13 contains the normalized B-Scans of each defect indicating the rate of decrease in amplitude as the transducer is rotated. Figure 4-14 represents the normalized B-Scan incorporating the average reflected amplitude inspected from each defect.

Table 13: Defect angle test results

Defect Size	Average 6 dB drop angle (°)	6 dB drop angle standard deviation (°)
3/8" Slot	7.08	1.44
3/4" Slot	5.14	0.56
1.5" Slot	4.45	0.32

The angles associated with 50% maximum amplitude of each defect are listed in Table 13. Table 13 also indicates the standard deviation of each angle at which 50% maximum amplitude was attained. These results indicate that the reflected amplitude decreases at a slower rate with smaller defects than with

larger defects. The 50% drop in maximum amplitude associated with the 3/8"

slot was 7.08°, and the 50% amplitude associated with the 1.5" slot was 4.45°.

The results from this test could be used to account for human error in the

AWS ultrasonic testing code's acceptance criteria. Because the reflected

amplitude is an important component to the acceptance criteria, a conservative

amount of rotation should be assumed in acceptable indication ratings. If a

human error factor or acceptable rotation is identified at 4.5°, then the required

reflected amplitude in the acceptance criteria should account for a decrease in

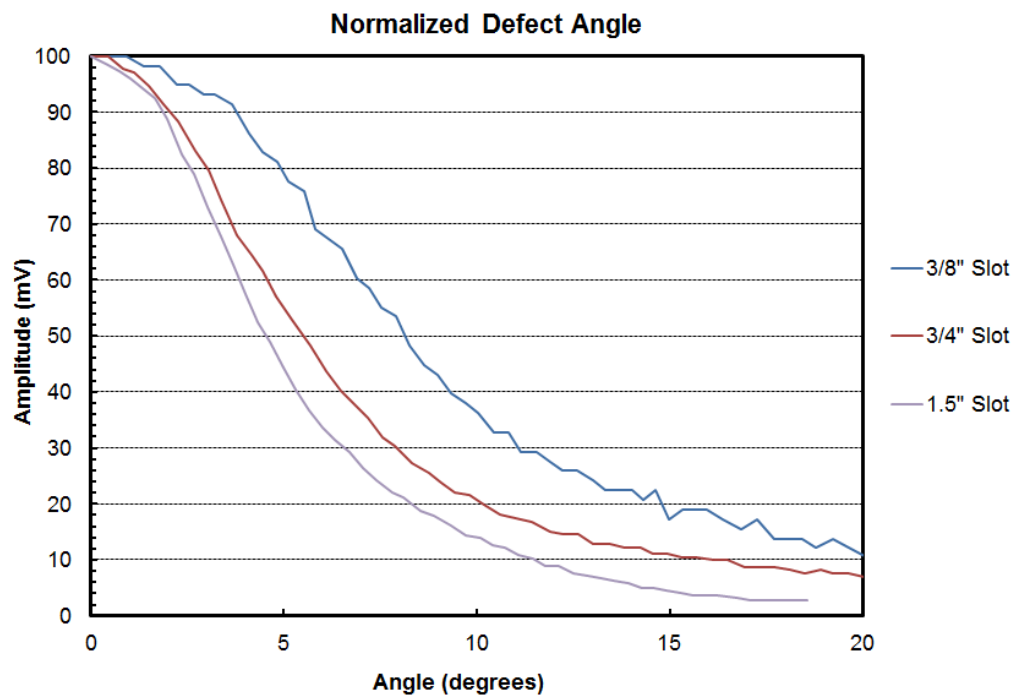reflected amplitude of a rejectable defect by 50%.

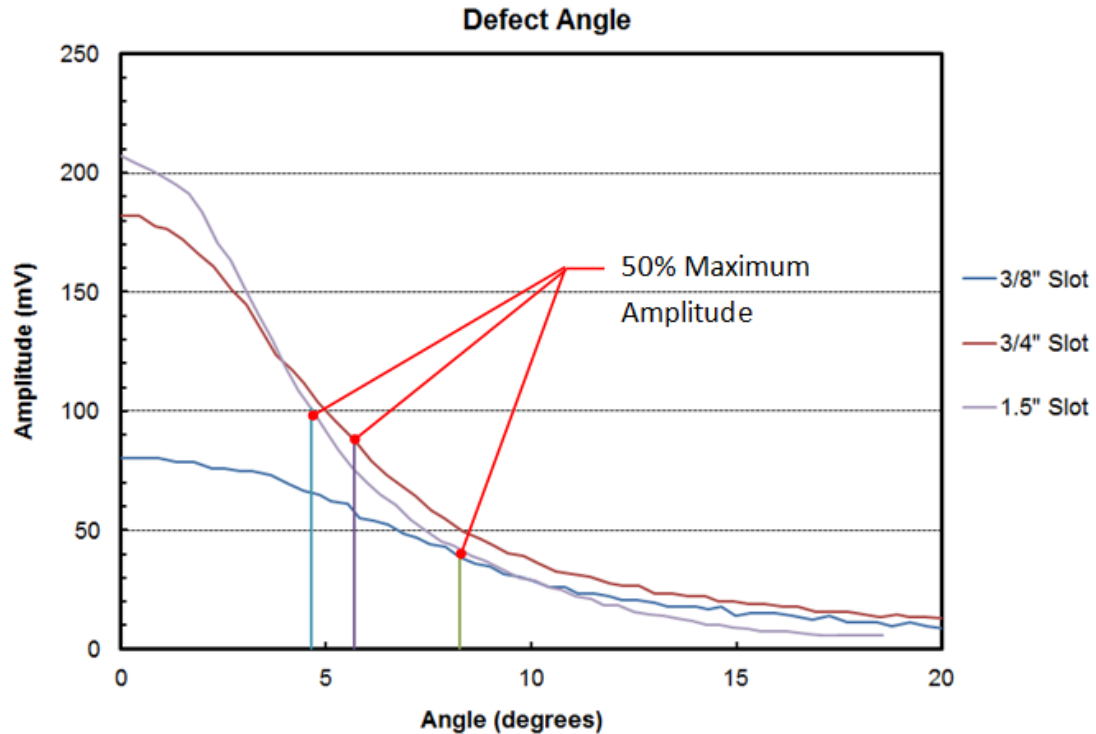**Figure 4-13: Normalized defect angle test B-Scans**

Figure 4-14: Reflected amplitude as the transducer is rotated about the defect

4.1.6 Transducer Angle

The transducer angle measurement test determined the amount of reflected amplitude lost due to transducer rotation about a focal point located within the transducer. Unlike the defect orientation, the focal point of rotation is located on the transducer. The rotation during this test moves the ultrasonic wave over the entire defect. The transducer orientation measurements were taken by inspecting the flat surfaces of the 1/4" and 1/8" FBH's located in the FBH1 plate as well as the bottom corners of the 3/8", 3/4", and 2.5" slots in the LA1 plate. The 1/32" and 1/16" FBH's in the FBH1 specimen were inspected, but the holes were too small for the transducer to identify. Due to the near field

interference in the first leg of the waveform, the bottom of the flat bottom holes were inspected within the second leg of the waveform.

In each of these inspections, the angle beam transducer was rotated while maintaining its location on the steel plate. An encoder was attached to the probe and was used to track the transducer's rotation. Each test yielded a B-Scan relating the reflected amplitude to the transducer angle. Figure 4-15 shows the normalized B-Scans of each inspection relative to the calculated transducer angle.

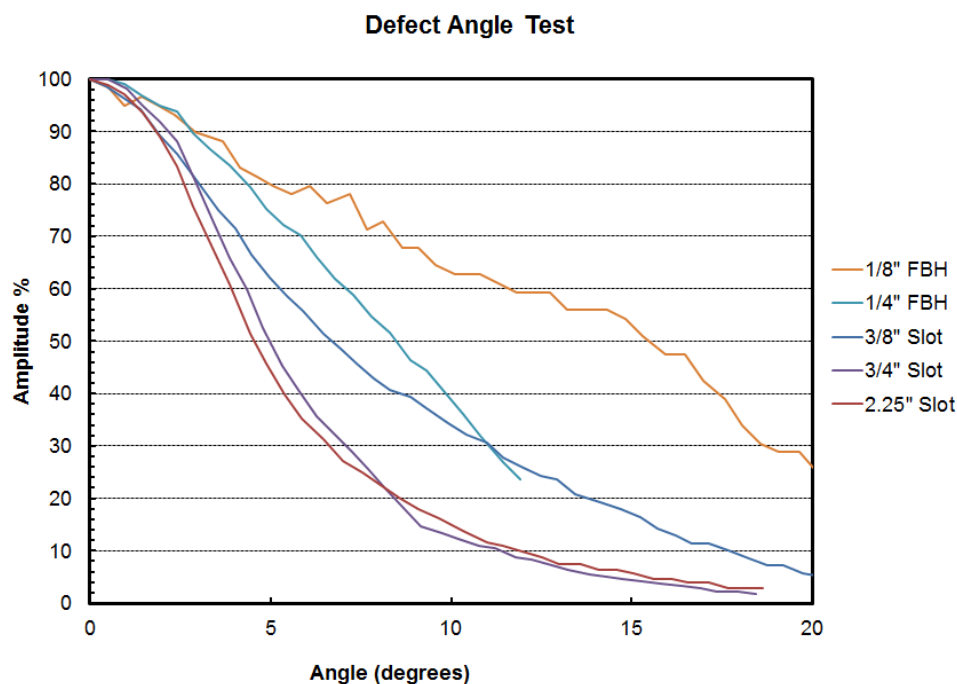**Defect Angle Test**

Figure 4-15: Normalized B-Scans relative to transducer rotation

The results in Table 14 indicate that the amplitude decreases rapidly when evaluating large defects and decreases gradually when evaluating small defects much smaller than the transducer. The results for the 1/8" FBH indicate a 50% decrease in reflected amplitude as the transducer was rotated by an average

84

angle of 12.8° with a standard deviation of 1.5°. The results for the 1/4" FBH indicate a 50% decrease in amplitude at an average angle of 11.1° with a standard deviation of 2.0°. These results indicate that the reflected amplitude decreases at different angles based on the diameter of the FBH's. These results show that the reflected wave drops more severely as the hole diameter increases.

Table 14: Transducer angle test results

Defect Size	Wave Path Length	Average 6 dB drop angle	6 dB drop angle standard deviation
1/8" FBH	3.3	12.8	1.5
1/4" FBH	3.3	11.1	2.0
3/8" Slot	2.9	6.2	0.4
3/4" Slot	2.9	5.1	0.3
2.25" Slot	2.9	4.6	0.2

Due to the relatively small size of the flat bottom holes, the 3/8", 3/4" and 2.5" slots of the LA1 plate were also inspected. The results of these inspections are shown in Table 14. The results show that defects larger than the transducer are impacted similarly as the transducer rotates. The B-Scans for the 3/8" in Table 14 show that the amplitude decreases to 50% when the transducer was rotated by an average angle of 6.2° with a standard deviation of 0.4°. The results for the 3/4" show that the amplitude decreases to 50% when the transducer was rotated by an average angle of 5.1° with a standard deviation of 0.3°. The results for the 2.25" show that the amplitude decreases to 50% when the transducer was rotated by an average angle of 4.6° with a standard deviation of 0.2°. These results were within 1.4° of each other, indicating that the transducer rotation does

not change based on the size of the flat slots. The results indicate that the reflected amplitude drops by 50% within at least 6.2° of transducer rotation.

The combined results from the FBH and LA1 holes indicated that the reflected amplitude decreases due to the size of the defect. Small defects such as the 1/8" diameter FBH may see a 6 dB decrease in amplitude after 13° of rotation, but larger defects such as the LA1 slots see a 6 dB decrease in amplitude after 5° of rotation. As the defect sizes increase, the reflected amplitude decreases at a faster rate. This discrepancy is consistent with beam spread effect seen in the length amplitude and beam spread tests.

Similar to the defect orientation tests, the transducer angle tests could be used to quantify human error during inspection. These tests show that the reflected amplitude will drop by 50% within at least 4.6°. If an acceptable rotation of 4.6° is assumed, then the acceptance code should be adjusted to account for 50% decrease in reflected amplitude of a rejectable defect.

4.1.7 Wedge Angle Test

The wedge angle test determined the decrease in reflected amplitude due to the incidence angle of each wedge angle. As described in Section 3.1.7, two procedures were used to determine the impact that the incidence angle of each angled wedge has on the reflected amplitude. The first procedure inspected the large horizontal pattern texture of the SR1 plate, Side 7 using each angled probe to relate the reflected amplitude of a vertical defect to the incidence angle. The second procedure inspected the bottom corners of the 1/16" diameter hole, the

3/8" slot, and the 3/4" slot in the LA1 test specimen using each of the three angle beam probes.

As described in Section 3.1.7, the AWS code adjusts the allowable reflected amplitude in the acceptance criteria based on the angle of incidence for the probe used during the inspection. The code assumes each indication represents a vertical crack within the steel because a vertical orientation is the most severe crack alignment. In order to replicate a vertical crack, the horizontal texture of SR1, Side 7 was inspected using each angle beam probe. Each probe was placed at the appropriate distance to inspect the same wall area located 1.25" deep on the SR1, Side 7.

Table 15: Wedge angle results from the SR1, Side 7 inspections

Angle	Average Amplitude	dB Change
45°	29.4	8.4
60°	58.8	2.4
70°	77.2	0.0

The results in Figure 4-16 and Table 15 identify the average reflected amplitude and the decibel adjustment required to translate the average amplitude to the 70° amplitude. These results do not agree with the assumptions in listed in Section 3.1.7. Table 4 in Section 3.1.7 indicates that the AWS code requires a 3 dB increase in sensitivity to relate an indication from a 60° probe to an indication using a 70° probe. It also shows a 5 dB increase in sensitivity to relate an indication from a 45° probe to an indication using a 70° probe. The results from

this test indicate that 8.4 dB and 2.4 dB are required to adjust the 45° and 60° probe indications, respectively.
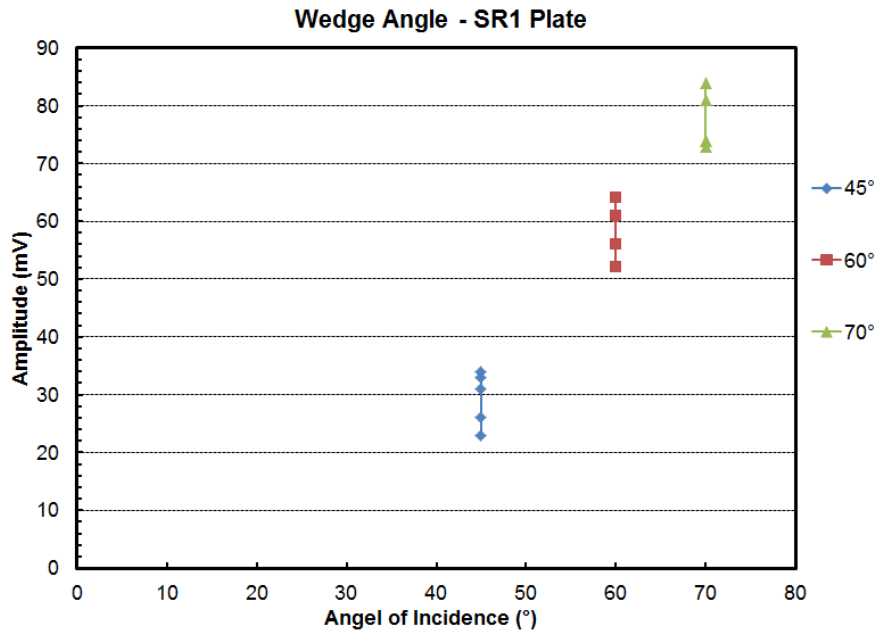

Figure 4-16: Maximum amplitudes from the SR1, Side 7 using the 45°, 60° and 70° wedges

The second procedure inspected the bottom corners of the 1/16" diameter hole, the 3/8" slot and the 3/4" slot in the LA1 test specimen using each of the three angle beam probes. While the AWS assumes all cracks are vertically oriented, this is not always the case. The bottom corners were chosen to demonstrate the effect that the defect orientation has on all three transducer wedge results.
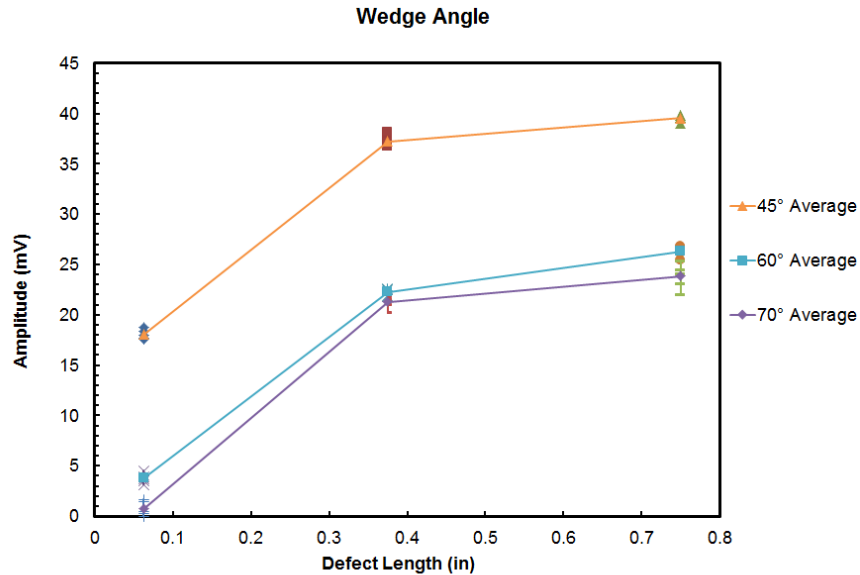
Figure 4-17 Wedge angle results relative to the smallest reflected amplitude

The results shown in Figure 4-17 and Table 16**Error! Not a valid bookmark self-reference.** indicate that a smaller angle of incident is associated with larger reflected amplitudes when inspecting the slot corner. Figure 4-17 and Table 16 relate all measured reflected amplitudes to the smallest reflected amplitude measured at 81 mV at a gain measurement of 62.   The 45° probe reflected an average amplitude 14.3 dB, 14.9 dB and 13.3 dB larger than the reflected amplitude of the 60° probe.   The 60° probe reflected an average amplitude 3.1 dB, 1 dB and 2.5 dB larger than the 70° probe.

Table 16: Wedge angle test results from the slot corner inspections

Wedge Angle	Average Reflected Amplitude		
	1/16" Hole	3/8" Slot	3/4" Slot
45°	18.1	37.2	39.6
60°	3.8	22.3	26.3
70°	0.7	21.3	23.8

These test results indicate that the most efficient inspection angle is not the horizontal beam assumed in the AWS code. Defects with similar orientations may have been rejected using a 45° probe, but not rejected using the other two angle beam probes. It may be more effective to inspect the weld with multiple angles and establish a single amplitude threshold for acceptance or rejection.

4.1.8 Defect Length Measurement

The defect length measurement tests determine the effectiveness of the current AWS length measurement technique when inspecting realistic flaws. The SMB 11 plate was inspected to identify and characterize the three defects embedded within the weld. B-Scans were developed during the inspection of each SMB-11 defect and used to determine each defects' length. The encoder tracked the movement of the probe as the transducer acquired waveforms. The locations at which the amplitude dropped by 50% represent the defect edges and are used to establish the measured length.

The AWS code requires that each weld is inspected from multiple sides and the largest amplitude and length measurements are recorded. For this research, each defect was inspected from all four sides of the weld: side A+, side A-, side B+, and side B-. Side A+ refers to the initial face (A) of inspection and the initial side (+) of the weld. Side B- refers to the opposite face (B) of inspection and on the opposite side (-) of the weld. Due to Defect 3's location at the bottom of the weld, the defect was inspected within the second leg of the

wave path; the remaining defects were inspected within the first leg of the wave path.

The results in Table 17 display the length measurements for all three defects inspected at all four sides of the weld. The length measurements for all defects vary between each inspection side. For example, the Defect 3 consists of a 0.4" toe crack extending across the bottom of the plate. The defect was measured on the first leg from Face A+ and Face A-. These inspections yielded length measurements near or slightly undersized of the actual length. The defect had to be inspected at the end of the second leg during the Face B+ and Face B- inspections due to the position of the defect within the weld. These inspections yielded overestimated length values. This length overestimation is due to the effect of beam spread on a defect smaller than the transducer as seen in the length measurement tests.

Table 17: Defect Length test results

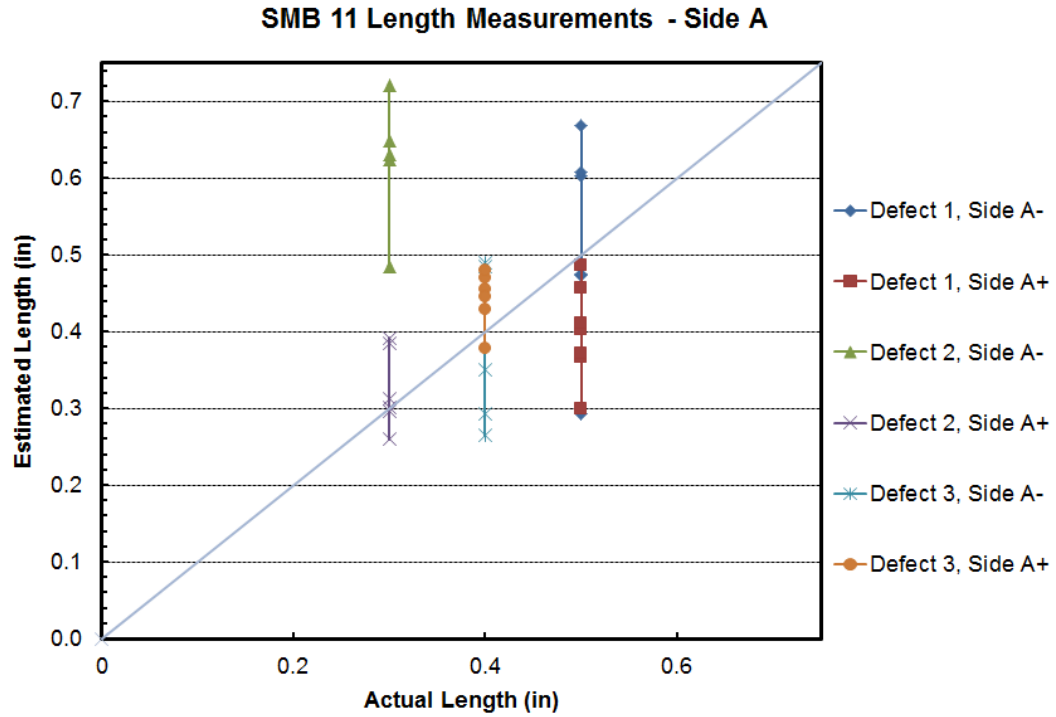| Defect Size	Average Measured Length			
	Face A+	Face A-	Face B+	Face B-
0.3"	0.62	0.32	0.40	0.45
0.4"	0.38	0.44	0.64	0.63
0.5"	0.52	0.40	0.77	0.53

Figure 4-18: SMB 11 Length measurements from Face A+ and Face A-
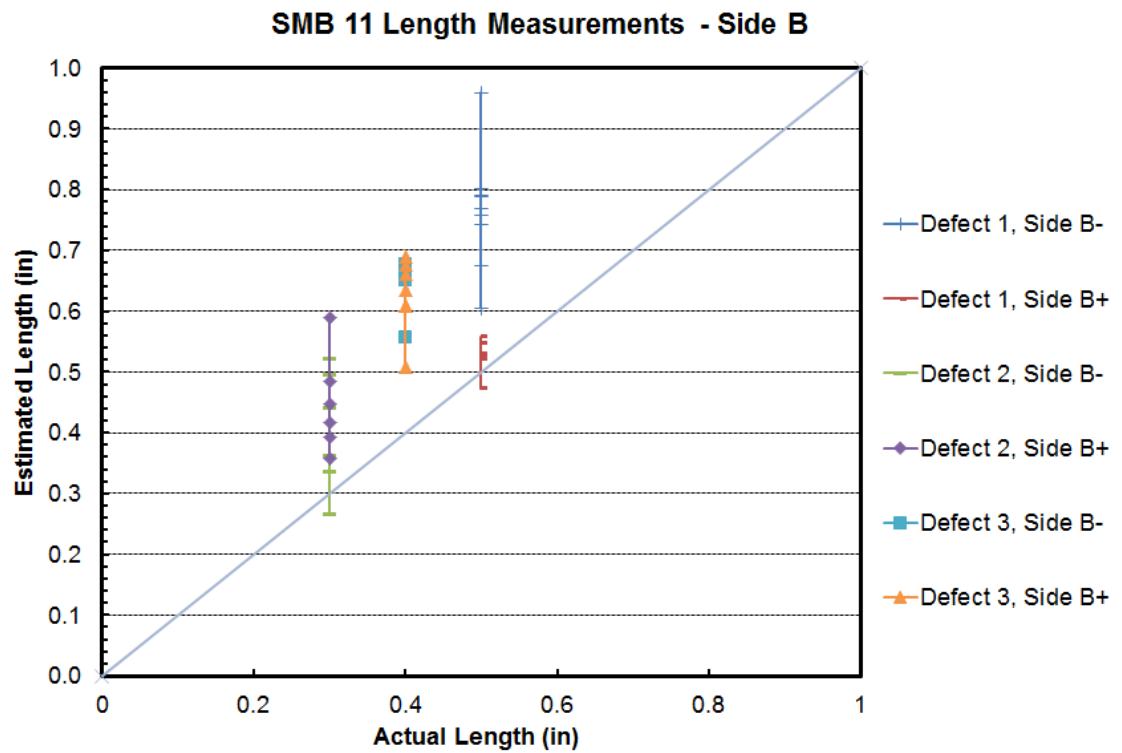

Figure 4-19: SMB 11 Length measurements from Face B+ and Face B-

4.2 Phased Array Ultrasonic Testing

This section describes the use of PAUT and demonstrates its unique defect characterization features. As described in Section 2.1.2, PAUT incorporates multiple element arrays to rapidly generate waves of constructive interference at multiple angles. The reflected waves are organized and displayed in S-Scan similar to the image in Figure 4-22.
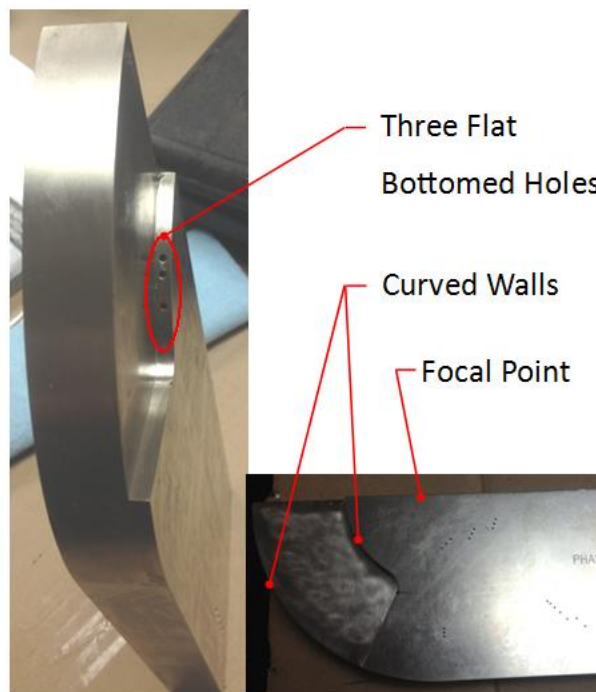

Figure 4-20: Phased Array IIW Block

The phased array IIW block shown in Figure 4-20 was inspected using a Phasor XS, PAUT pulser receiver. The phased array IIW block contains two curved walls of different radices whose focal point is identified in Figure 4-20. Three flat bottom holes are located on the interior curved wall. These flat bottom holes are difficult to identify using a standard UT A-Scan; however, the PAUT S-Scan clearly identifies the three circular holes as seen in Figure 4-22.
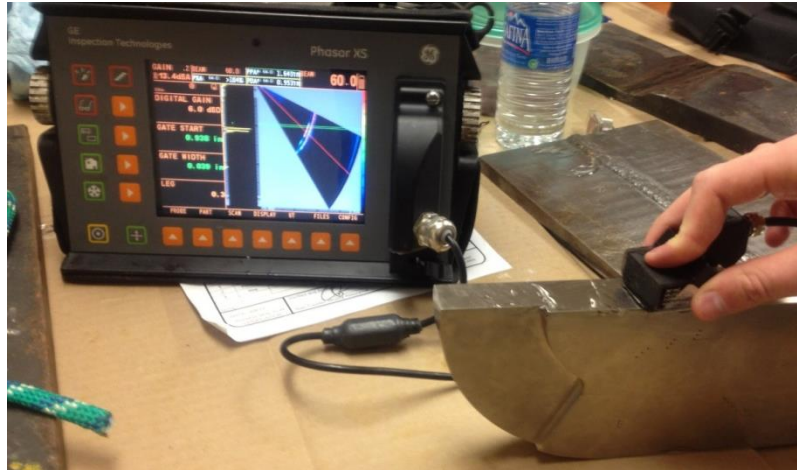
Figure 4-21: PAUT inspection of the phased array IIW block

This scan incorporated a 32 element PAUT transducer to create a 40°-75° S-Scan. In order to identify both curved walls and all three flat bottom holes, the transducer was placed at the focal point of both curved walls on the IIW block as seen in Figure 4-21.

The Phasor XS receiver is capable of generating an A-Scan at any angle within the current angle range. The S-Scan in Figure 4-22 displays the A-Scan at 60° to the left of the S-Scan. The A-Scan angle is associated with the thin slanted line extending from the upper left-hand corner to the bottom right-hand corner of the S-Scan. The A-Scan at 60° shows three spikes in amplitude, the flat bottom hole (1), the first curved wall (2), and the second curved wall (3). Using the range of angles in a single inspection, each indication can be identified as a hole or a curved wall.
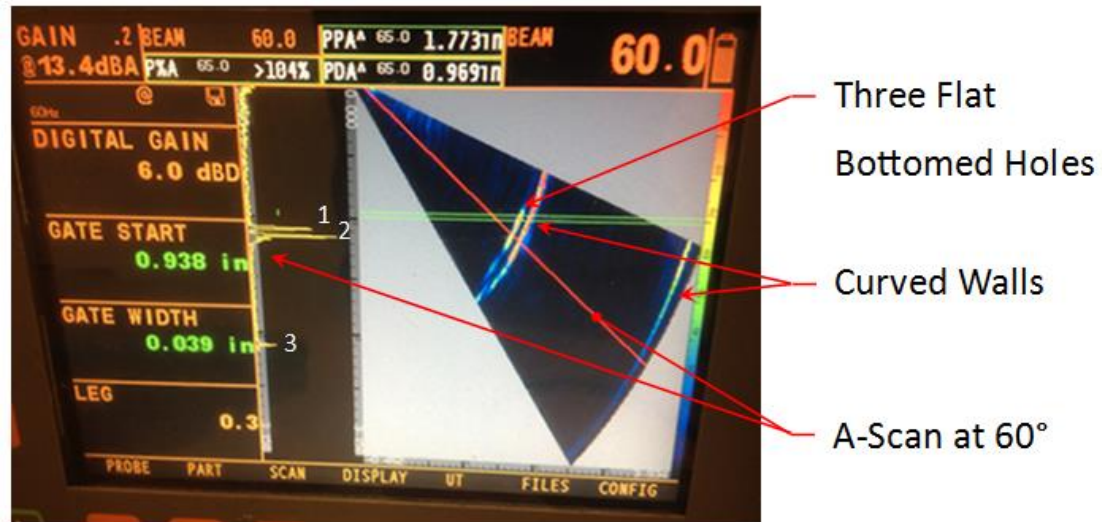
Figure 4-22: S-Scan of the PAUT IIW block

These characterization features provided in an S-Scan may entice inspectors toward using PAUT rather than UT. Defects similar to the flaws located in the SMB11 may be easier to identify as well as characterize. Planar defects similar to the cracks in the SMB 11 may be oriented at less than optimal orientations for a single A-Scan angle; however, the PAUT incorporates a large range of angles that encompass the other optimal inspection angles. Volumetric defects such as porosity resemble regions of reflected amplitude in an S-Scan. Depending on the significance of these amplitudes, the defect may be overlooked using a traditional A-Scan. The test procedures in Appendix C are to be performed to identify and compare the common limitations of both UT and PAUT. These limitations should be considered when developing a PAUT procedure for bridge and building inspection.

5 CONCLUSIONS

The objectives of this research were to measure the impact of variables that affect the ultrasonic response, to evaluate the current UT procedure, to improve upon the UT procedure based on the measured results and to develop test procedures that measure the variables that impact PAUT measurements for future research.

This chapter summarizes the results from the procedures described in Chapter 3 and Chapter 4 that identified and quantified the variables that affect ultrasonic test the measurements. These procedures evaluated the acoustic beam characteristics, including beam spread, attenuation, wedge angle and transducer orientation. Other procedures evaluated defect characteristics, including defect orientation and defect texture. The remaining test procedures assessed the UT testing procedure used to detect and characterize defects within steel welds by evaluating the length measurements of both fabricated slots in test specimens and defects within a steel weld. These tests measured the variables that impact the reflected amplitude and length measurement used in ultrasonic testing to identify and characterize defects within steel welds. The results were then compared to the assumptions made in the current AWS ultrasonic testing procedure. Data analysis from the experimental measurements has yielded the following results:

- The defect orientation test found that the reflected amplitude dropped by 6 dB within a minimum transducer rotation of 4.45° about the defect.

- The wedge angle measurements found that the amplitude decreased as the beam incidence angle decreased. The results do not agree with the AWS acceptance criteria assumptions, and indicate that maximum reflected amplitude is determined by the defect orientation within the weld and the beam's incidence angle.

- The length measurement tests results indicated that defects larger than the transducer were accurately sized but that defects smaller than the transducer were oversized. The extent to which these smaller defects were oversized increased as the path length increased due to beam spread.

- The beam spread measurements found that the length measurements for slots smaller than the transducer increased as the measured wave path length increased due to the effect of beam spread. The beam spread effect increased as the slot length decreased for slots smaller than the transducer. The length measurements for slots larger than the transducer were not influenced by beam spread.

- The attenuation measurements found that the amplitudes decreased by a maximum of 8.06 dB over an increase in wave path length of 2.926". The amplitude decreased more for smaller defects than for larger defects. An additional test was conducted which inspected the SR1, Side 7 wall at different wave path lengths. The results found that the reflected amplitude dropped by 4.25 dB/in rather than 2 dB/in assumed by the AWS ultrasonic testing code.

- The defect texture measurements indicated that the reflected amplitudes from the fatigue specimens were best represented by the horizontal patterns of the SR1 plate. The results also show that the maximum reflected amplitude varied greatly for each texture inspection.

- The transducer orientation measurements identified the amount of amplitude lost as the transducer was rotated while remaining at the same x-y coordinates. The results indicated that the reflected amplitude decreased by 6 dB with a minimum rotation of 4.6°.

The defect length measurements assessed the current length measurement procedure by evaluating fabricated defects within a welded steel specimen. Each defect was inspected from both sides of the weld, on both faces of the plate. The results found that the orientation at which the defect was inspected caused the length measurements from each inspection location to be inconsistent. The results showed that the defects were typically oversized, but the measured lengths were further overestimated when inspected from longer wave path lengths.

- The next portion for this project will conduct these test procedures using phased array ultrasonic testing. These procedures evaluate the following: Beam Spread, Attenuation, Transducer Orientation, Length Measurement, Defect Texture, Defect Orientation and Defect Length. These procedures are detailed in Appendix B, including what to inspect, how to analyze the data and how to compare the results to the UT results.

The results from these UT tests indicate that the current AWS ultrasonic testing procedure may need to be adjusted to better represent the behavior of the UT technology. The reflected amplitude is a critical component used to indicate the severity of the defect; however, these tests indicate that the reflected amplitude is affected by the beam angle, defect texture, transducer orientation, and the attenuation by the material. The length measurement is the other key component in ultrasonic inspection, but it is limited by factors which include transducer oscillator length, beam spread, and defect position within the weld.

The results from both ultrasonic and phased array ultrasonic testing will be compared to develop a phased array procedure used to inspect steel welds. The variables measured in this research and measured in future research should be accounted for in the PAUT procedure. The results from this research suggest the following be considered for PAUT inspection:

- Defects representing the acceptance threshold for the AWS. The defects should consist of different textures, such as rough fatigue cracks, smooth slag inclusions, etc. The reflected amplitude from these defects should be used to develop the acceptance criteria. The defect texture test results from this research indicated that the reflected amplitude is affected by the defect roughness. Currently, the AWS UT procedure does not account for the defect's texture. By evaluating similarly sized defects containing various textures, the acceptance criteria will better represent severe defects.

- The inspection code should include measurements from actual defect reflections to develop a curve that accounts for material attenuation, similar to a DAC curve. The results from the attenuation tests indicate that the 2 dB/in assumption is inaccurate. The most effective way to measure attenuation would be to measure defects of the same size at multiple distances. The size of these defects should resemble the threshold for acceptance or rejection. Any defect indication larger than the created DAC curve is rejected.

- Instead of adjusting the indication acceptance criteria based on a vertical crack, the PAUT inspection should use an amplitude value that is applied to all inspection angles. The wedge angle tests indicated a change in amplitude based on the wedge angle and the defect orientation. All cracks are inspected at multiple angles and the maximum reflected amplitude from the defect would be identified using one of the various angles in a PAUT S-Scan. This maximum amplitude should be compared to accepted reflected amplitude rather than an amplitude based on an angle.

- Defects with measured lengths equaled to the transducer length should be further evaluated during the inspection process to avoid length overestimation. The length measurement, beam spread, and defect length tests indicate that defects with lengths shorter than the transducer are susceptible to overestimation due to beam spread effects and the transducer length encompassing the defect as shown in Figure 3-1.
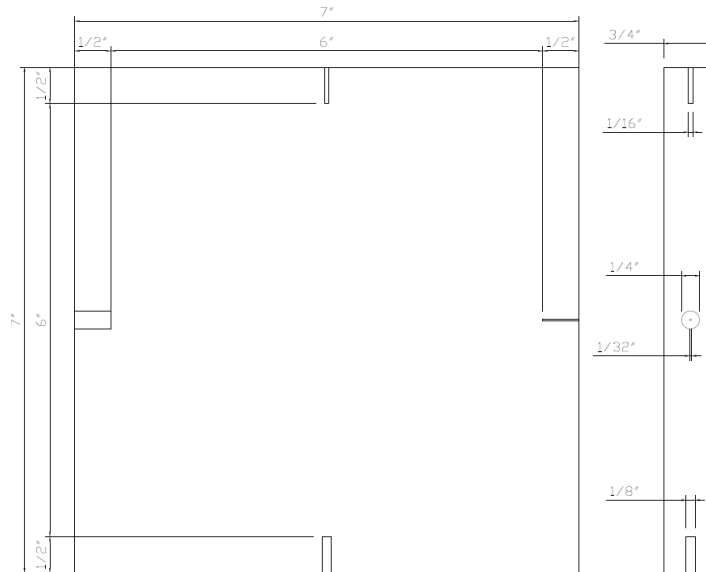
100

APPENDIX A – SPECIMEN INFORMATION

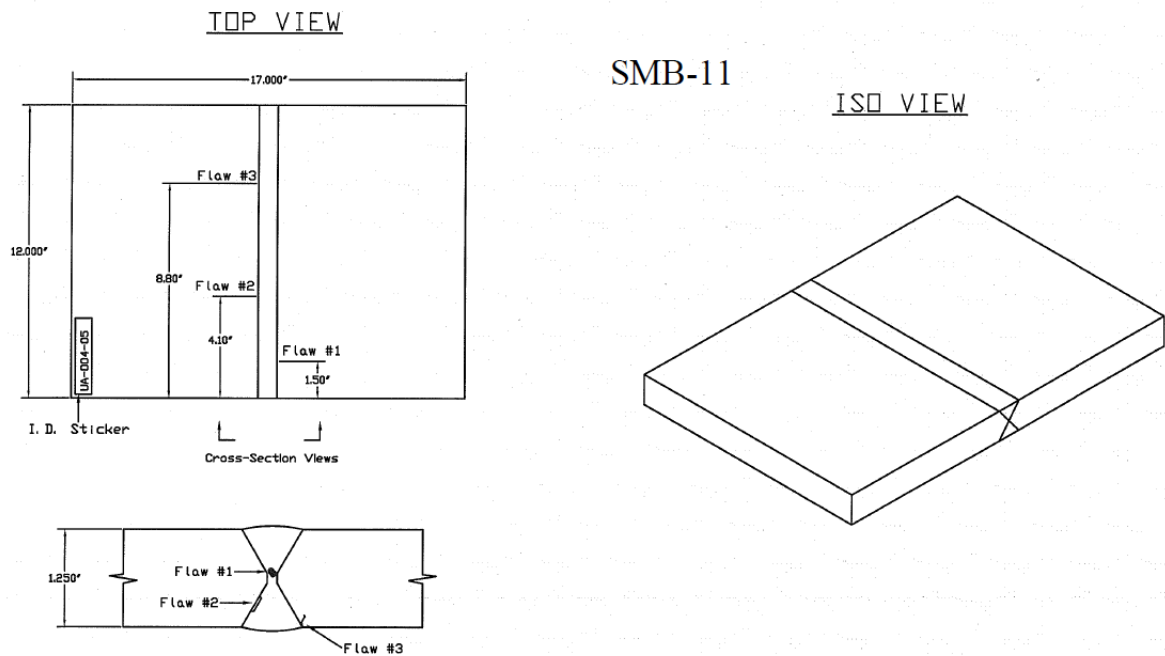
Figure A-1: Flat Bottom hole specimen

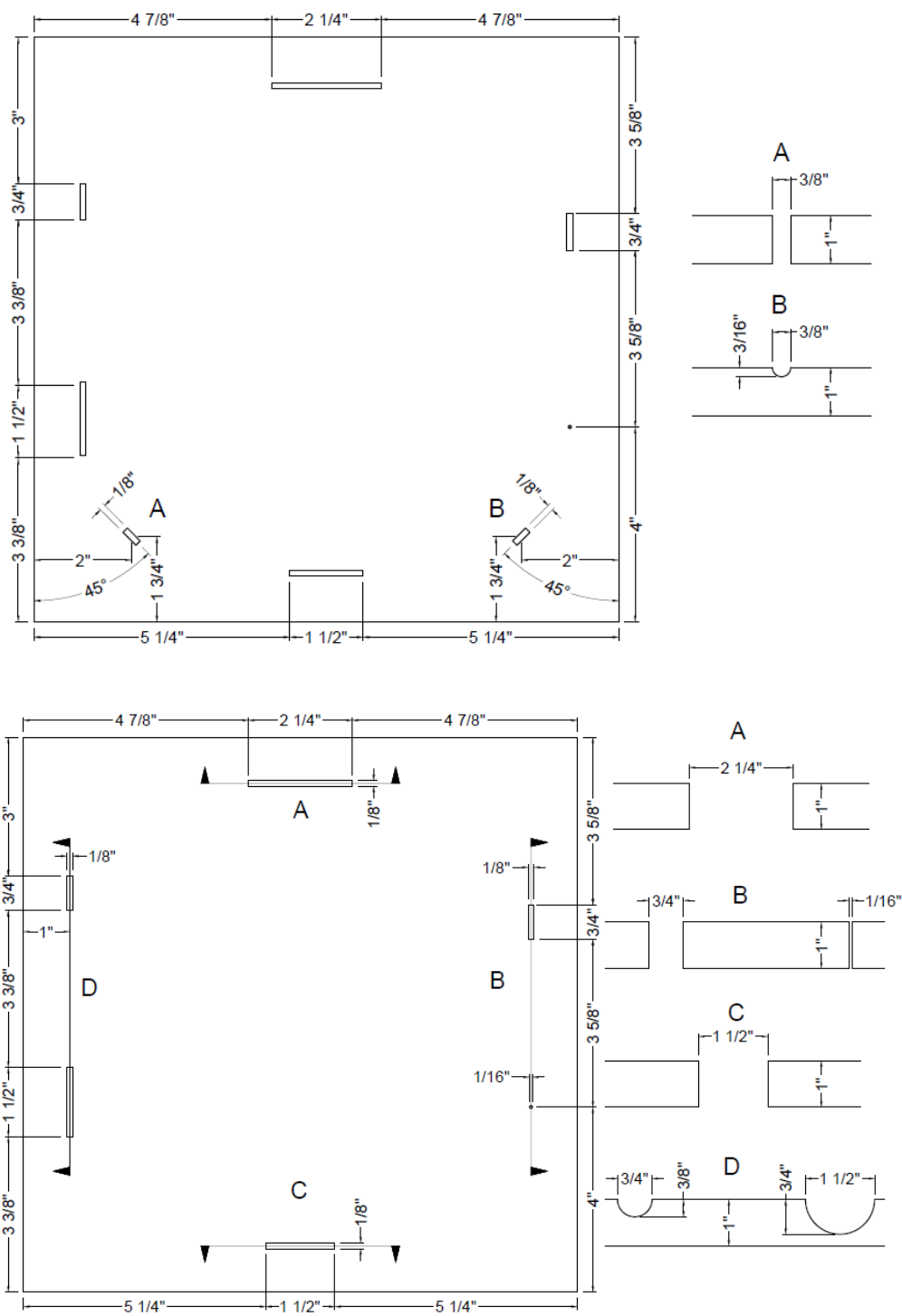**Figure A-2: Details depicting the SMB 11 plate defect locations**

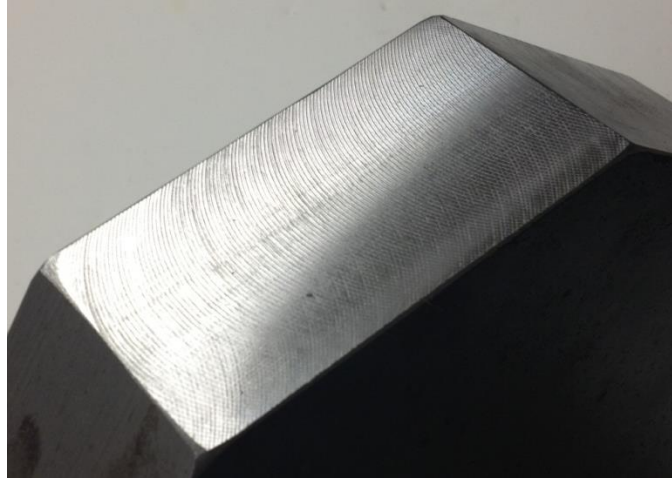**Figure A-3: Length-amplitude specimen design drawing**

Figure A-4: Surface roughness specimen: small profile finish
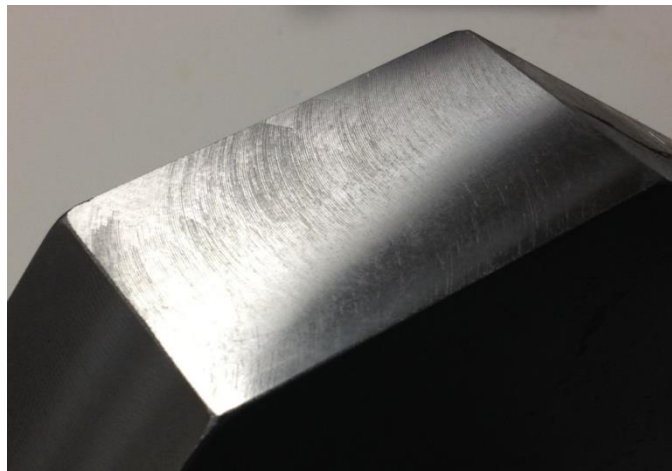

Figure A-5: Surface roughness specimen: fine finish

Figure A-6: Surface roughness specimen: medium profile finish

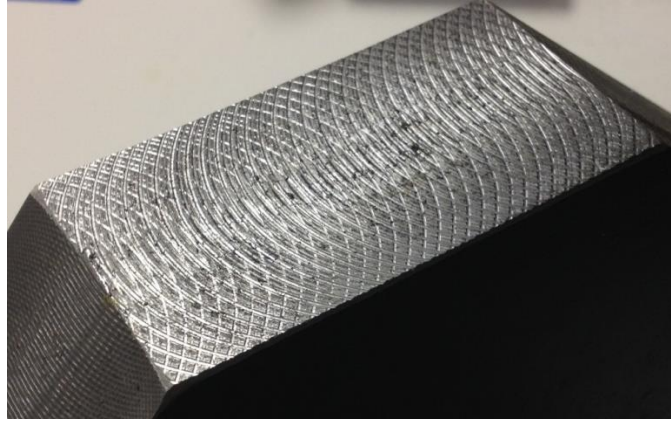**Figure A-7: Surface roughness specimen: large profile finish**
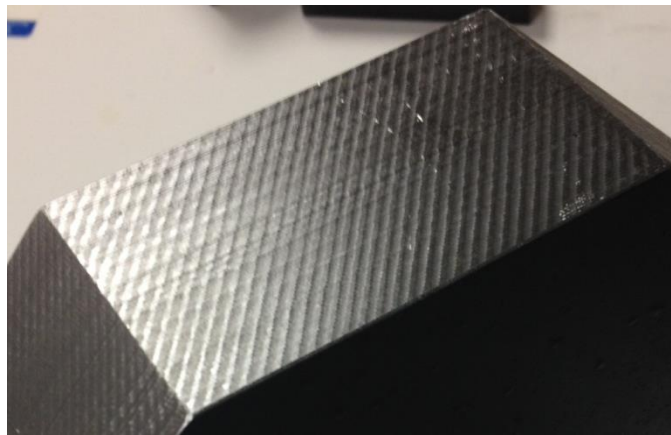
Figure A-8: Surface roughness specimen: small horizontal finish
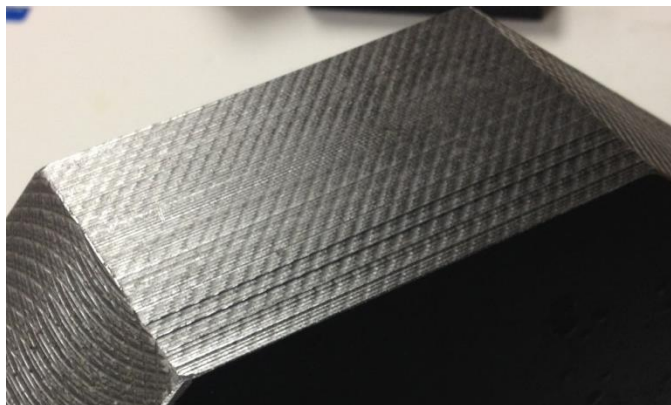
Figure A-9: Surface roughness specimen: large horizontal finish

Figure A-10: Surface roughness specimen: manufacture cut finish

Figure A-11: SR Fatigue Specimen 1

Figure A-12: SR-Fatigue Specimen 1-Side 1

Figure A-13: SR-Fatigue Specimen 1-Side 2

Figure A-14: SR-Fatigue Specimen 1-Side 3

Figure A-15: SR-Fatigue Specimen 1-Side 4

Figure A-16: SR-Fatigue Specimen 1-Side 5

Figure A-17: SR-Fatigue Specimen 2-Side 6

APPENDIX B – PAUT PROCEDURES
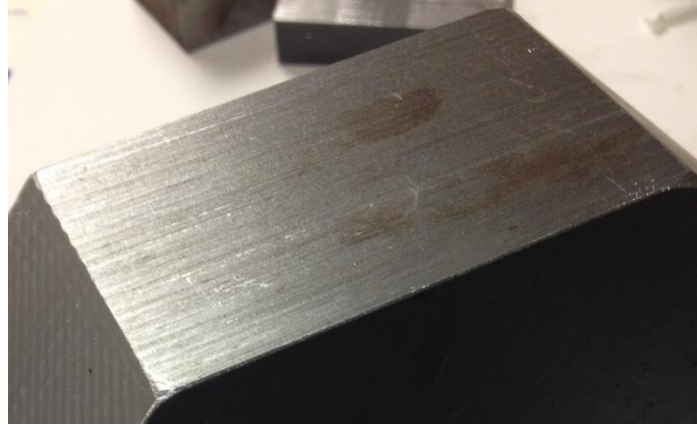
This section describes the test procedures used to evaluate the variables that influence PAUT measurements. The variables identified in Chapters 3 and 4 for UT will be evaluated using the procedures described in this appendix. The procedures include what is defects or components are inspected, how to assess the measured data and how these data relate to the results collected from the UT tests to develop a procedure to inspect welds in steel components using PAUT.

B.1 Phased Array Ultrasonic Testing Transducer Settings

This section describes the PAUT settings used during each inspection including the angle range of the S-Scan, the gain settings and the encoder collection rate. Each inspection should produce either a single S-Scan or multiple S-Scans associated with a location using an encoder. Similar to the B-Scans used in the UT measurements, a region based on wave path length within an angle range should be evaluated for each encoded S-Scan as shown in Figure B-1. The maximum amplitude from this region will be associated to an encoder location. The resulting data will provide figures similar to the B-Scans shown in Figure 3-5 created during the UT inspections.

Each series of tests should be evaluated using the same sensitivity, or gain. If the gain needs to be adjusted during inspection, the sensitivity change needs to be accounted for in the data analysis.

The encoder collection rate used during these tests needs to be as high as allowable. During the UT measurements, the encoder was set at

approximately 0.0232" per scan to accurately measure the location. If the rate was set any higher, the encoder would not record the data before the next scan started. The PAUT encoder acquisition rate should be set to maximize the number of S-Scans over a given inspection path without causing interruption from the next location's reading.
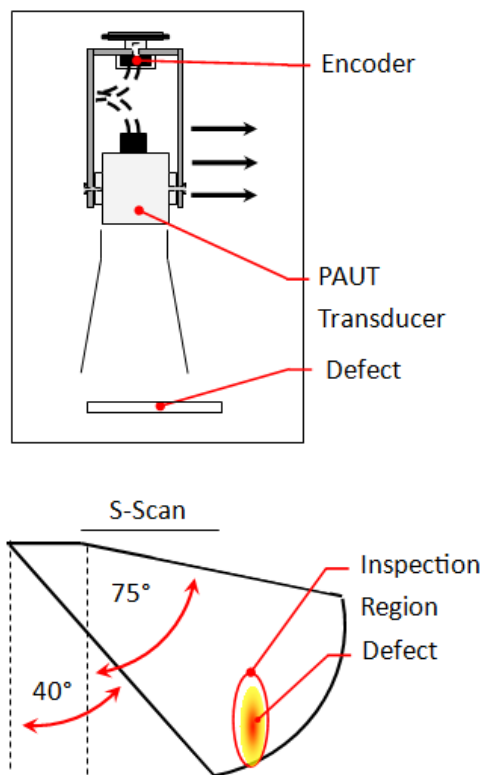

Figure B-1: Diagram of S-Scan inspection region

B.2 Surface Texture

The defect texture measurement evaluates the reflected amplitude from specimens containing different wall surface finishes. In order evaluate subsurface discontinuities with known textures, the SR1 containing walls with

different surface finishes are inspected. The SR1 shown in Figure A-4 to Figure A-10, contains 7 sides with different surface finishes.

B-Scans were developed in the UT portion to acquire the largest reflected amplitude from each inspected side; however, the PAUT may not require encoded S-Scans. Ten S-Scans inspecting the same texture should be adequate to characterize each side. The inspected region should identify the maximum reflections from the textured walls. The maximum reflected amplitude from each inspection should show the change in reflected amplitude due to the inspected side's texture. The changes in reflected amplitude from the PAUT results should be considered when developing the acceptance criteria for the PAUT inspection.

B.3 Length Amplitude

The length measurement test evaluates the accuracy of the 6 dB drop technique defined in the AWS code to measure defects using PAUT. In order evaluate discontinuities with known lengths, the LA1 plate was manufactured with 8 electric discharge machined (EDM) defects of different lengths and geometries. The transducer should inspect each slot on Leg 1, at the bottom edge of the slot and on Leg 2, at the top edge of the slot. Both legs are inspected to evaluate the difference between length measurements and the actual slot size and to determine the beam spread effect at a longer wave path length. The defects' edges are associated with a 6 dB drop in amplitude. The

111

measured length of each defect is the distance between the measured edges of both defect sides.
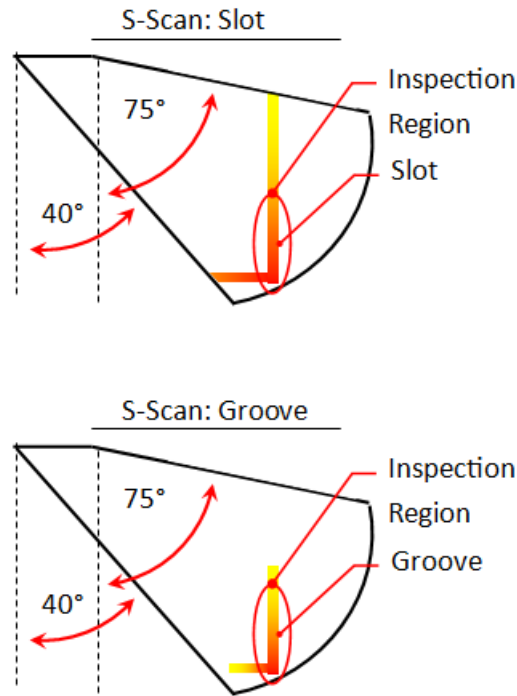

Figure B-2: Predicted S-Scan measurements of LA1 plate slot and groove defects

Each S-Scan should consist of the maximum reflected waves from each slot or groove. When analyzing the data, be sure to identify any differences between the groove and slot reflections. It is expected that the groove reflections should reflect similar maximum amplitudes but at fewer angles as seen in Figure B-2. The groove reflections should reflect the acoustic wave at fewer angles in each encoded S-Scan inspection; whereas the slots should reflect angles throughout the entire slot depth in each encoded S-Scan inspection. The groove measurements should compare to fatigue cracks found in the field. The results should also indicate the impact beam spread has on the measured length of

112

each defect. If the 6 dB drop technique is not adequately measuring the length of the defects, then a different procedure should be considered in the PAUT procedure.

B.4 Defect Orientation

The defect orientation test measures the reflected amplitude as the transducer is rotated about the face of a defect.   The maximum reflected amplitude measured during the inspection occurs when the defect is oriented perpendicular to the transducer.   This test will provide data identifying the decrease in amplitude due to the defect orientation relative to the transducer. The data can be used to identify an acceptable angle at which in-situ defects can be inspected.

This test evaluates the 3/8", 3/4" and 1.5" slots from the LA1 plate to determine the effect of the defect angle on different sized defects. Each defect should be inspected at the bottom of the first leg. Figure B-3 shows the test setup used to focus the acoustic wave on a single focal point throughout each inspection.   Mounting tape was used to connect the transducer to the flat aluminum connection. The connection remained stationary using a bolt and a magnet as seen in Figure B-4
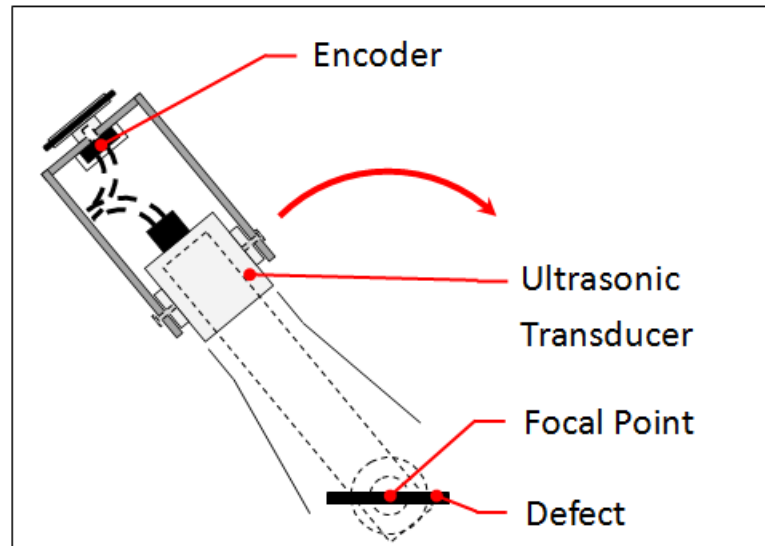
Figure B-3: Defect Angle test setup diagram
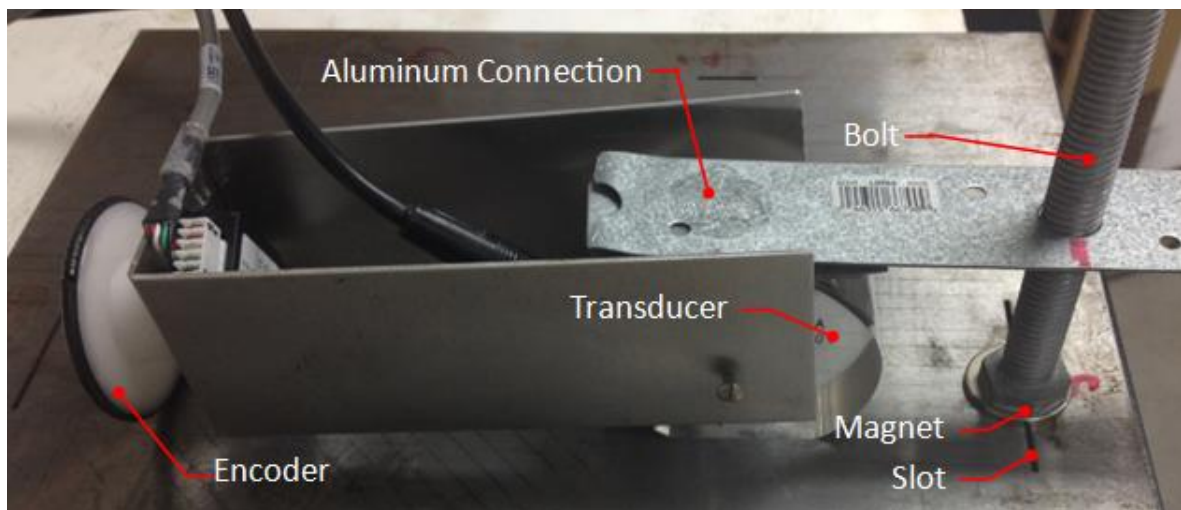
Figure B-4: Defect Angle test setup

The connection shown in Figure B-4 was used to maintain a constant distance from the defect while focusing the ultrasonic transducer to a focal point. This focal point was placed at the center of each defect. As the transducer was positioned at different angles relative to the defect, the encoder attached to the transducer tracked its location. The rotation values were calculated from the

encoder location points. The results relate the maximum reflected amplitude of the inspected region of each S-Scan to the rotation values calculated from the encoder location points. The results from these measurements can then be used to identify an appropriate human error factor applied to the PAUT defect acceptance criteria.

B.5 Transducer Rotation

The transducer rotation test evaluate the reflected amplitude as the transducer was turned while remaining in the same X-Y coordinates. This test looks to determine the amount of reflected amplitude received by the transducer as the wave is rotated away from the defect. The bottom corners of the 3/8", 3/4" and 2.25" slot will be inspected using the setup shown in Figure B-5 and Figure B-6.
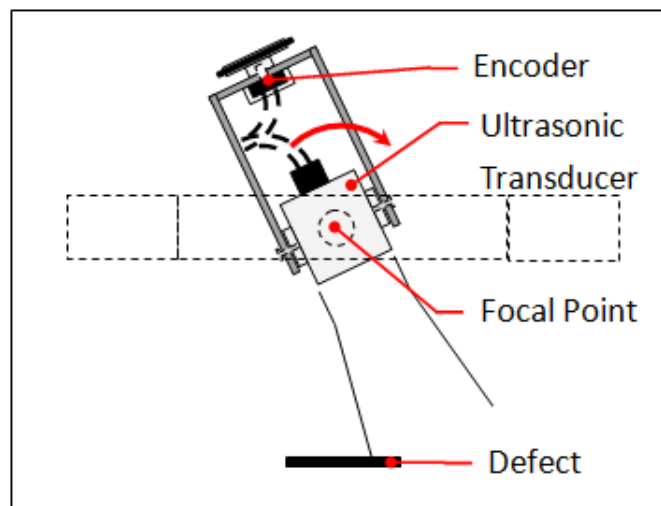

Figure B-5: Transducer rotation test setup diagram

Figure B-5 shows the connection used during the UT inspections. A similar connection design should be used during the PAUT measurements.

Figure B-5 shows the flat top bolt that around which the transducer rotated was glued to the top of a thin aluminum plate. The thin aluminum plate was connected to the transducer using sufficient mounting tape to eliminate excess movement between the aluminum plate and the transducer. The steel frame was placed on the bolt to maintain the same X-Y coordinates as the transducer rotated. The bolt maintains the probe's location but also allows the transducer to turn.
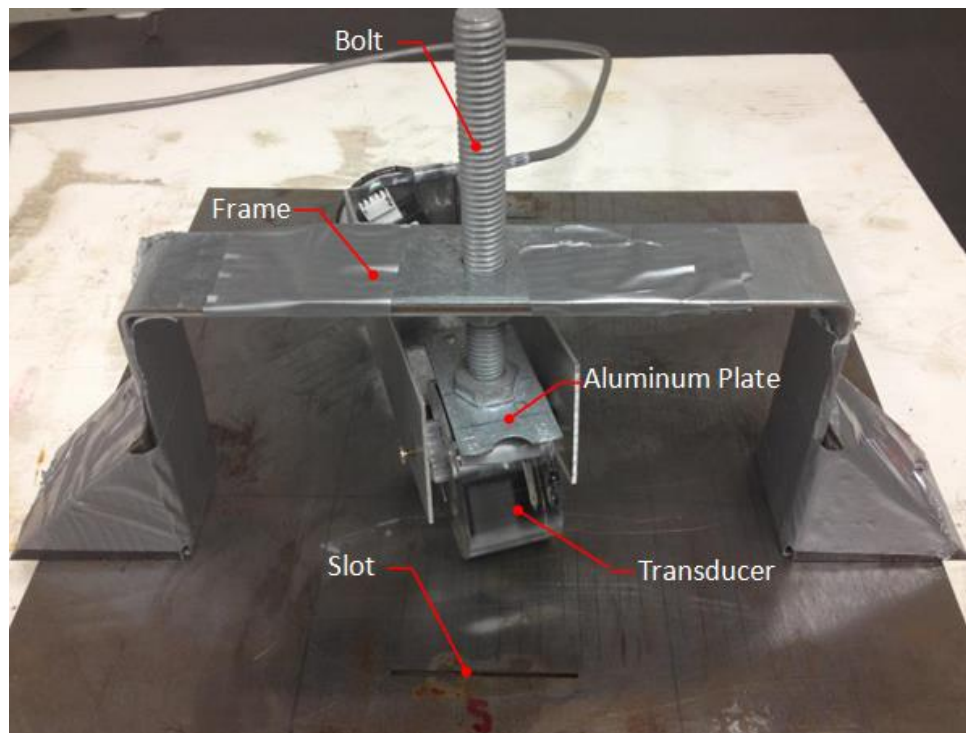

Figure B-6: Transducer rotation test setup

The transducer rotation tests require the acoustic wave to move on and off the defect. This movement is not required in the defect angle test. As the transducer was rotated, the encoder attached to the transducer tracked the location. The rotation values are then calculated from the encoder location

points.   The resulting graphs relate the transducer rotation to the maximum reflected amplitude from the S-Scan inspection regions.

The results from this procedure should be used to determine an acceptable angle at which the transducer can be rotated when inspecting defects.   Even the slightest transducer rotation can dramatically affect the reflected amplitude.   The PAUT procedure should apply a human error factor to the acceptance criteria that accounts for the loss of reflected amplitude due to an acceptable transducer rotation angle.

B.6 Beam Spread

The beam spread test evaluates the effect beam spread has on the length measurement.   This test looks to identify the beam spread angle for slots both shorter and longer than the transducer length.   These tests measure the lengths of the 1/16", the 3/8" and the 3/4" slot in the LA1 plate at different wave path lengths.   The results from the length measurements will be used to determine the effect of beam spread on the length measurement as the wave path length increases.   These defects were chosen for the UT measurements to evaluate defects both longer and smaller than the transducer length.   The PAUT probe has a different transducer length and the length measurements could be affected by beam spread differently.

The length measurements from the encoded S-Scans were developed to show the reflected amplitude relative to the transducer location. The encoded S-Scans were initially taken at a surface distance of 1.75" away from each slot.

Each scan was conducted after moving the transducer away from the slot at 1/4"

increments to a maximum of a 6" surface distance. The inspected zone should

inspect the bottom corner of each defect to determine the edges of each slot.

These edges are identified with a 6 dB drop in amplitude. The lengths are then

compared to the wave path lengths at which the encoded S-Scans were taken.

These lengths may increase as the wave path lengths increase due to the defect

size and the effect of beam spread.

The results from this procedure are used to determine the beam spread

effect on different defect lengths. Ultrasonic testing uses a different probe with

different size transducers which possibly alter the beam spread impact. The

beam spread impact needs to be identified for PAUT to determine if the test

procedure needs to include additional measurement requirements for smaller

defects.

B.7 Attenuation Factor

The attenuation tests evaluated the reflected amplitude as the wave path

length increases. As the wave travels through the material, the wave energy is

scattered and absorbed as the acoustic wave propagates through the material.

The AWS ultrasonic testing code accounts for this energy loss by reducing the

amplitude by 2 dB for every inch of wave path length. Other codes such as the

ASME and API codes incorporate the DAC curve. This research looks to

determine if the 2 dB assumption is accurate.

The data for the attenuation tests should be collected from the encoded S-Scans measured during the beam spread tests. The maximum reflected amplitude from each S-Scan is recorded and compared to the inspection distance. The top and bottom corners of each LA1 slot reflect the highest amplitudes; however, these amplitudes are not similar due to the change in wave path length. These corners provide ideal attenuation measurements because they are similar in geometry and are inspected at different wave path lengths.

An additional test was performed to evaluate the effect of attenuation. This test evaluated the large horizontal pattern on the Side 7 of the SR1 plate at multiple distances to generate results similar to a Distance Amplitude Correction (DAC) curve. This test assumes that the roughness is constant throughout the wall area and that the roughness of the SR1 wall reflects constant amplitudes over the wall area. This wall was chosen to replicate a defect that spans over the entire wall surface and can be evaluated at different wave path lengths. The decrease in reflected amplitude due to a attenuation at each wave path length is then compared to the 2 dB AWS assumption.

This test evaluated the SR1 plate with the horizontal pattern plate at multiple distances. In order to avoid the near field interference, the transducer was placed a distance of 1.5" away from the side. The transducer is then moved back 1/4" until a distance of 4" is attained. A-Scans are taken at each distance and the wall reflection is recorded. These reflections are then organized to generate results comparing the measured reflected amplitude to the wave path length at the time of inspection.

Most DAC curves in the ASME and API only evaluate 3 to 4 defects to establish a curve; this test evaluates 13 locations with different wave path lengths. By including more locations, a curve would not have to be assumed. These locations should identify the reflected amplitude from the same defect at different depths. Multiple reflections should provide a better representation of the attenuation for the entire waveform. These results should be used to develop a factor or procedure similar to the DAC for PAUT inspections that accounts for the loss of reflected amplitude due to attenuation.

B.8 Defect Sizing

The defect sizing test evaluates manufactured defects within steel welds using the AWS sizing procedure. Instead of evaluating steel specimens with fabricated slots, this test sizes realistic defects using the 50% amplitude drop similar to the AWS ultrasonic procedure. The effectiveness of the AWS sizing technique can be more accurately evaluated by inspecting realistic defects in fabricated welds rather than EDM slots.

This test evaluates the three fabricated defects located in the weld of the SMB-11 plate. Each defect should be inspected on both faces of both sides. The root crack (Defect 3) must be inspected on both the first and second leg of the wave path due to its location at the bottom of the weld. This provides a great example of the beam spread effect on the length measurement. This test inspects every defect from every angle and compares the length measurements. Encoded S-Scans will be developed to determine the length measurement for

each defect. After the defect is identified, the transducer should be oriented perpendicular to the weld and moved parallel to the weld.   The reflected amplitude is evaluated to determine the 6 dB drop location associated with the defect edge.   The measured defect length is associated with the distance between the two defect edges.

The results from this test should be used to assess the effectiveness of PAUT in evaluating defects within steel welds using the current AWS procedure. If the length measurements from the PAUT tests are affected by beam spread, then the PAUT procedure needs to account for its limitation.

REFERENCES

ASME (2011). "2010 ASME Section V Nondestructive Examination."

ASTM (2008). Standard Guide for Magnetic Particle Testing.

ASTM (2009). Standard Practice for Contact Ultrasonic Testing of Welds Using Phased Arrays.

ASTM (2010). Standard Guide for Radiographic Testing.

ASTM (2012). Standard Test Method for Liquid Penetrant Examination.

ASTM (2013). Evaluating Performance Characteristics of Phased-Array

Ultrasonic Examination Instruments and Systems. E-2491-13.

AWS, D. (2010). "D1. 1/D1. 1M-Structural Welding Code-Steel." American Welding Society.

Bridge Welding Code, A. (2010). "AASHTO/AWS D1.5M/D1.5:2010 BRIDGE WELDING CODE." American Association of State Highway and Transportation Officials.

Charlesworth, J. P. and J. A. G. Temple (1989). Engineering applications of ultrasonic time-of-flight diffraction, Research Studies Press Somerset.

Crutzen, S., P. Lemaitre and I. Iacono (1996). Realistic defects suitable for ISI capability evaluation and qualification. 14 th International Conference on NDE in the Nuclear and Pressure Vessel Industries.

Curie, J. and P. Curie (1880). "Piezoelectric and allied phenomena in Rochelle salt." Comput Rend Acad Sci Paris **91**: 294-297.

Desch, C., D. Sproule and W. Dawson (1946). "The detection of cracks in steel by means of supersonic waves." Journal of the Iron and Steel Institute **153**(1): P319-P321.

Ditchburn, R. and M. Ibrahim (2009). Ultrasonic Phased Arrays for the Inspection of Thick-Section Welds, DTIC Document.

Firestone, F. A. (1942). Flaw detecting device and measuring instrument, US Patent 2,280,226.

Gorrill, G. W. (2011). BRIDGE INSPECTION REPORT-SHERMAN MINTON BRIDGE I-64 OVER THE OHIO RIVER SPANS 1, 2, A, B AND C STATE OF INDIANA DEPARTMENT OF TRANSPORTATION.

Gruber, G. J. and G. M. Light (2002). "Supplemental Ultrasonic Code Inspection of Structural Weldments." Journal of materials in civil engineering **14**(1): 57-61.

Hotaki, H. and G. Washer (2014). COMPARISON OF NONDESTRUCTIVE TESTING TECHNOLOGIES USED FOR INSPECTION OF WELDED JOINTS OF HIGHWAY STEEL BRIDGES. Master of Science, University of Missouri.

Jessop, T. J., P. J. Mudge and J. D. Harrison (1981). "Ultrasonic measurement of weld flaw size." NCHRP Report(242).

Krautkrämer, J. and H. Krautkrämer (1990). "Ultrasonic testing of materials."

Lamarre, A., M. Moles and V. Lupien (2000). Phased array ultrasonic inspection of friction stir weldments. REVIEW OF PROGRESS IN QUANTITATIVE NONDESTRUCTIVE EVALUATION: Volume 19, AIP Publishing.

Meyer, H.-J. (1984). "The international state of the art in nondestructive inspection of welds with special emphasis on flaw caracterization." Materials evaluation **42**(6): 793-802.

Moore, M., B. M. Phares and G. A. Washer (2004). Guidelines for Ultrasonic Inspection of Hanger Pins.

Murthy, B. (1998). "Radiation Protection In Industrial Radiography."

Nagy, P. B. and J. H. Rose (1993). "Surface roughness and the ultrasonic detection of subsurface scatterers." Journal of applied physics **73**(2): 566-580.

Ogilvy, J. (1989). "Model for the ultrasonic inspection of rough defects." Ultrasonics **27**(2): 69-79.

Rana, M. D., O. Hedden, D. Cowfer and R. Boyce (2001). "Technical basis for ASME Section VIII Code Case 2235 on ultrasonic examination of welds in lieu of radiography." Journal of pressure vessel technology **123**(3): 338-345.

Shaw Jr, R. E. (2002). "Ultrasonic Testing Procedures, Technician Skills, and Qualifications." Journal of materials in civil engineering **14**(1): 62-67.

Silk, M. (1977). Sizing crack-like defects by ultrasonic means.

Song, S.-J., H. J. Shin and Y. H. Jang (2002). "Development of an ultra sonic phased array system for nondestructive tests of nuclear power plant components." Nuclear engineering and design **214**(1): 151-161.

Standard, A. (2005). "1104–Twentieth Edition,"." Welding of Pipelines and Related Facilities," American Petroleum Institute, Washington, DC.

Stone, M. and M. Green (2011). Sherman Minton problems will take 3 weeks to diagnose, officials say. The Courier-Journal.

Washer, G., R. Connor and D. Looten (2013). "Performance Testing of Inspectors Implementing NDT Technologies." TRB.

Wilkinson, S. and S. M. Duke (2014). Comparative Testing of Radiographic Testing, Ultrasonic Testing and Phased Array Advanced Ultrasonic Testing Non Destructive Testing Techniques in Accordance with the AWS D1. 5 Bridge Welding Code.

Wirdelius, H. and E. Österberg (2000). "Study of defect characteristics essential for NDT testing methods ET, UT and RT." SKI Project(98267): 3.